Supporting Information

Photoinduced Electron Transfer Coupled to Donor Deprotonation and Acceptor Protonation in a Molecular Triad Mimicking Photosystem II

Andrea Pannwitz and Oliver S. Wenger*

Department of Chemistry, University of Basel, St. Johanns-Ring 19, 4056 Basel, Switzerland

Table of contents

Synthesis and product characterization

All synthesis steps were performed under nitrogen atmosphere. 2,5-Dimethyl-4-trimethylsilyl-1-phenylboronic acid (**2**) was synthesized from 2,5-dibromo-*p*-xylene according to an established published procedure.[1] Syntheses of phenols **3** and **4** were similar to previous work,[1] as well as the borylation yielding compound **5**,[2] and the synthesis of compound **7**,[3] and 13.[4] $[RuCl_2(bpy)_2]\cdot 2H_2O$ (**11**) was synthesized from 2,2'-bpy and $RuCl_3\cdot xH_2O$ as reported.[5] The synthesis of $MQPF_6$ has been reported previously.[6] All other chemicals used in this work are commercially available.

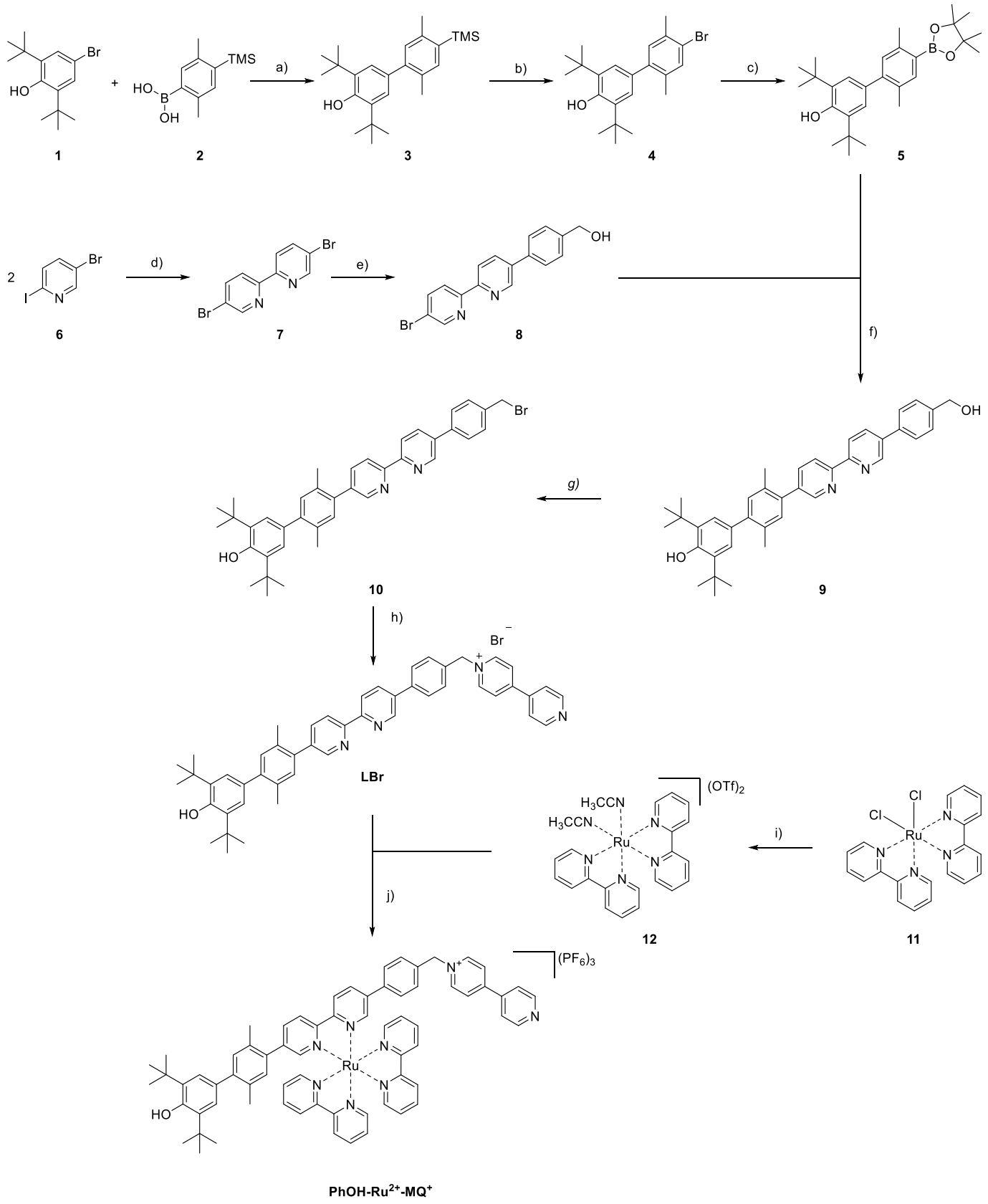

Scheme S1. Synthesis plan for the triad. a) $Pd(PPh_3)_4$, Na_2CO_3, THF/H_2O 8:1, reflux, dark 67 %, b) Br_2, NaOAc, THF, 0 °C, dark 68 %, c) $(BPin)_2$, $[PdCl_2(dppf)]\cdot CH_2Cl_2$, KOAc, DMSO, 100 °C, 86 %, d) bis(tributyltin), $Pd(PPh_3)_4$, *m*-xylene, 180 °C, <61%, e) 4-(hydroxymethyl)phenylboronic acid, K_2CO_3, $Pd(PPh_3)_4$, THF/H_2O 8:1, reflux, 39%, f) K_2CO_3, $Pd(PPh_3)_4$, THF/H_2O 5:1, reflux, 95%, g) PBr_3, dry CH_2Cl_2, room temperature, 89%, h) 4,4'-bpy, dry CH_2Cl_2, reflux, 59%, i) AgOTf, CH_3CN, reflux, ~100%, j) ethylene glycol, AgOTf, 105 °C, 90%.

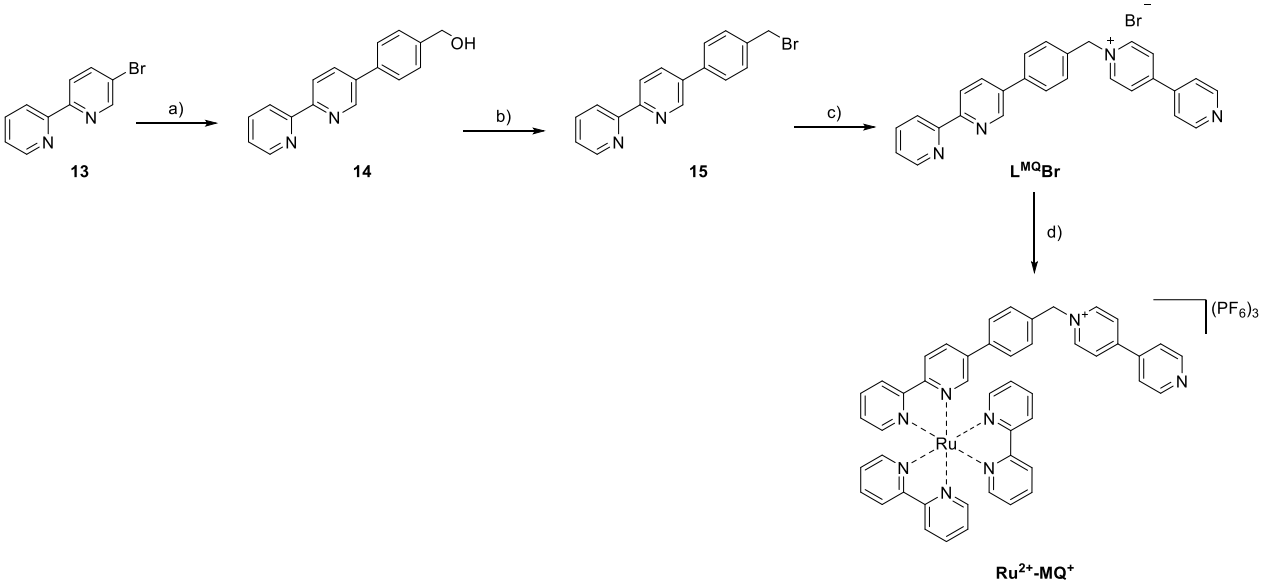

Scheme S2. Synthesis plan for the reference dyad. a) 4-(Hydroxymethyl)phenylboronic acid, K_2CO_3, $Pd(PPh_3)_4$, THF/H_2O 8:1, reflux, 71%, b) PBr_3, dry CH_2Cl_2, room temperature, 52%, c) 4,4'-bpy, dry CH_2Cl_2, reflux, 99%, d) ethylene glycol, AgOTf, 105 °C, 40%.

3,5-Di-*tert*-butyl-2',5'-dimethyl-4'-(trimethylsilyl)-[1,1'-biphenyl]-4-ol (3)[1]

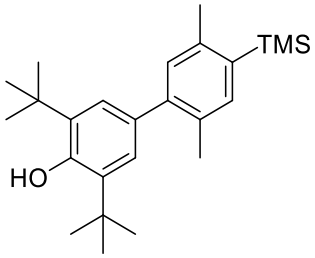

3

A mixture of 4-bromo-2,6-di-*tert*-butylphenol (**1**) (1.27 g, 4.45 mmol, 1.00 eq.), 2,5-dimethyl-4-trimethylsilyl-1-phenylboronic acid (**2**) (1.19 g, 5.18 mmol, 1.16 eq.), Na_2CO_3 (1.41 g, 13.3 mmol, 3.00 eq.), and $Pd(PPh_3)_4$ (277 mg, 223 µmol, 5.0 mol%) in a degassed mixture of THF (40 mL) and water (5 mL) were heated at reflux in the dark for 16 h. After cooling to room temperature, the mixture was extracted with CH_2Cl_2 (3×). The combined organic phases were dried over Na_2SO_4 and the solvent was removed under reduced pressure. Purification by column chromatography (SiO_2, pentane) afforded compound **3** as a colorless oil (1.14 g, 2.98 mmol, 67 %).

^{1}H NMR (400 MHz, $CDCl_3$): δ (ppm) = 7.35 (s, 1H), 7.14 (s, 2H), 7.08 (s, 1H), 5.19 (s, 1H), 2.46 (s, 3H), 2.28 (s, 3H), 1.46 (s, 18H), 0.35 (s, 9H).

^{13}C NMR (101 MHz, $CDCl_3$): δ (ppm) = 152.85, 143.59, 140.96, 136.76, 136.54, 135.46, 132.86, 131.73, 131.60, 126.00, 34.59, 30.59, 22.60, 20.38, 0.13.

4'-Bromo-3,5-di-*tert*-butyl-2',5'-dimethyl-[1,1'-biphenyl]-4-ol (4)[1]

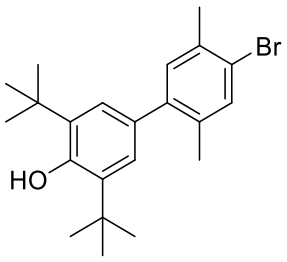

4

Bromine (1.3 mL, 4.2 g, 26 mmol, 4.1 eq.) was added to a degassed suspension of **PhOH-xy-TMS** (2.50 g, 6.42 mmol, 1.00 eq.) and NaOAc (1.07 g, 13.0 mmol, 2.03 eq.) in dry THF (40 mL) at 0 °C in the dark. The mixture was stirred in the dark at room temperature for 2.5 h, then NEt_3 (7.3 mL, 52 mmol, 8.0 eq.) and saturated aqueous $Na_2S_2O_3$ solution (55 mL) were added, and stirring of the black mixture was continued for 16 h. The mixture was extracted with CH_2Cl_2 (3×), the organic phases were dried over Na_2SO_4, and finally the solvent was removed under reduced pressure. Purification by column chromatography (SiO_2, pentane → pentane/CH_2Cl_2 1:3) afforded compound **4** as an off-white solid (1.71 g, 4.38 mmol, 68 %).

^{1}H NMR (400 MHz, $CDCl_3$): δ (ppm) = 7.43 (s, 1H), 7.11 (s, 1H), 7.08 (s, 2H), 5.22 (s, 1H), 2.39 (s, 3H), 2.23 (s, 3H), 1.47 (s, 18H).

^{13}C NMR (101 MHz, $CDCl_3$): δ (ppm) = 153.03, 142.07, 135.64, 134.98, 134.95, 133.83, 132.35, 131.97, 125.82, 122.97, 34.56, 30.54, 22.44, 20.12.

3,5-Di-*tert*-butyl-2',5'-dimethyl-4'-(4,4,5,5-tetramethyl-1,3,2-dioxaborolan-2-yl)-[1,1'-biphenyl]-4-ol (5)[2]

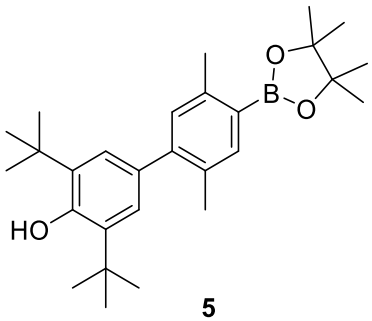

5

A mixture of compound **4** (1.65 g, 4.23 mmol, 1.00 eq.), bis(pinacolato)diboron (1.61 g, 6.33 mmol, 1.5 eq.) KOAc (1.66 g, 16.9 mmol, 4.00 eq.) and [$PdCl_2$(dppf)]·CH_2Cl_2 (172 mg, 211 µmol, 5 mol%) in DMSO (60 mL) was degassed and subsequently heated at 100 °C in the dark for 16 h. After cooling to room temperature, water and brine were added, and the mixture was extracted with pentane (3×). The combined organic phases were dried over Na_2SO_4, and the solvent was removed under reduced pressure. Purification by column chromatography (SiO_2, pentane / CH_2Cl_2 5:1) afforded compound **5** as a white solid (1.57 g, 3.62 mmol, 86 %).

^{1}H NMR (400 MHz, $CDCl_3$): δ (ppm) = 7.68 (s, 1H), 7.13 (s, 2H), 7.08 (s, 1H), 5.20 (s, 1H), 2.54 (s, 3H), 2.27 (s, 3H), 1.46 (s, 18H), 1.35 (s, 12H).

^{13}C NMR (101 MHz, $CDCl_3$): δ (ppm) = 152.77, 145.14, 142.27, 138.06, 135.32, 132.79, 131.57, 125.74, 83.30, 34.42, 30.42, 24.88, 21.70, 19.97.

5,5'-Dibromo-2,2'-bipyridine (7)[3]

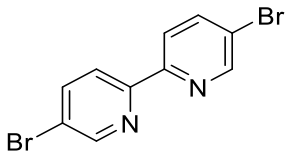

7

A mixture of 5-bromo-2-iodopyridine (**6**) (12.0 g, 42.3 mmol, 1.00 eq.), bis(tributyltin) (10.7 mL, 12.2 g, 21.2 mmol, 0.50 eq.) and *m*-xylene (60 mL) was degassed. After addition of $Pd(PPh_3)_4$ (977 mg, 785 µmol, 1.8 mol%) the reaction mixture was degassed again and heated at reflux for 3d. After cooling to room temperature, the solidified mixture was dissolved in CH_2Cl_2 and subjected to column chromatography (SiO_2, CH_2Cl_2). Compound **7** was isolated as an off-white solid (8.56 g, <25.9 mmol, <61%) that was contaminated with unidentified tin compounds (approximately 5 mol% based on ^{1}H NMR), as sometimes observed after Stille coupling reactions.

^{1}H NMR (400 MHz, $CDCl_3$): δ (ppm) = 8.70 (dd, *J* = 2.3, 0.8 Hz, 2H), 8.29 (dd, *J* = 8.4, 0.7 Hz, 2H), 7.93 (dd, *J* = 8.5, 2.4 Hz, 2H).

^{13}C NMR (101 MHz, $CDCl_3$): δ (ppm) = 150.19, 140.22, 122.72, 121.81.

(4-(5'-Bromo-[2,2'-bipyridin]-5-yl)phenyl)methanol (8)

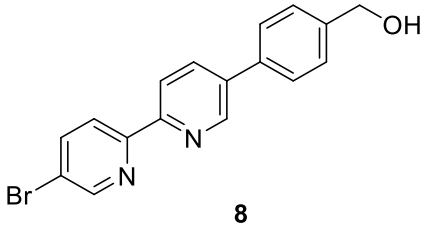

8

A mixture of compound **7** (870 mg, 2.77 mmol, 1.00 eq.), K_2CO_3 (1.15 g, 8.32 mmol, 3.00 eq.), THF (70 mL), and water (15 mL) was degassed. After addition of $Pd(PPh_3)_4$ (172 mg, 137 µmol, 5.0 mol%) the mixture was degassed again and heated to reflux. A degassed suspension of 4-(hydroxymethyl)phenylboronic acid (421 mg, 2.77 mmol, 1.00 eq.) in THF (55 mL) was added dropwise to the refluxing reaction mixture within 1 h. After the addition was complete, the mixture was heated for further 30 min and then cooled to room temperature. The mixture was extracted with CH_2Cl_2 (3×), and the combined organic phases were dried over Na_2SO_4, and then the solvent was removed under reduced pressure. Purification by column chromatography (SiO_2, CH_2Cl_2 → Et_2O) afforded unreacted starting material **7** (219 mg, 697 µmol, 25 %) and product **8** as a white solid (365 mg, 1.07 mmol, 39 %).

^{1}H NMR (400 MHz, $CDCl_3$): δ (ppm) = 8.91 (s, 1H), 8.75 (s, 1H), 8.48 (d, *J* = 8.3 Hz, 1H), 8.42 (d, *J* = 8.6 Hz, 1H), 8.06 (dd, *J* = 8.3, 2.3 Hz, 1H), 7.97 (dd, *J* = 8.5, 2.3 Hz, 1H), 7.65 (d, *J* = 8.2 Hz, 2H), 7.52 (d, *J* = 8.0 Hz, 2H), 4.79 (s, 2H), 1.83 (s, 1H).

^{13}C NMR (101 MHz, DMSO-d_6): δ (ppm) = 153.73, 152.89, 149.99, 147.27, 142.95, 139.90, 135.82, 134.97, 134.77, 127.16, 126.52, 122.08, 120.74, 120.42, 62.53.

3,5-Di-*tert*-butyl-4'-(5'-(4-(hydroxymethyl)phenyl)-[2,2'-bipyridin]-5-yl)-2',5'-dimethyl-[1,1'-biphenyl]-4-ol (9)

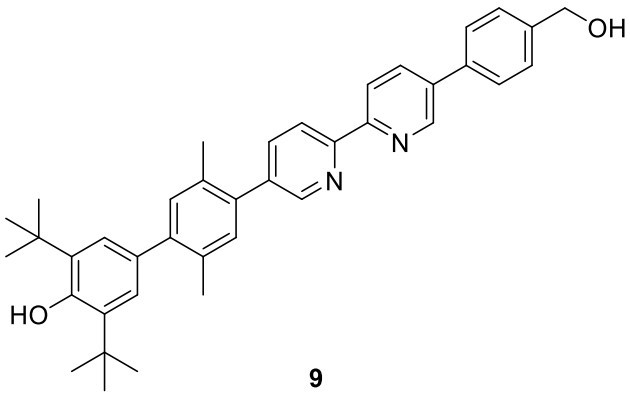

9

$Pd(PPh_3)_4$ (195 mg, 157 µmol, 5.0 mol%) was added to a degassed mixture of compound **8** (1.06 g, 3.11 mmol, 1.00 eq.), compound **5** (1.50 g, 3.44 mmol, 1.11 eq.) and K_2CO_3 (1.30 g, 9.41 mmol, 3.02 eq.), THF (100 mL), and water (20 mL). The reaction mixture was degassed again and subsequently heated to reflux for 15 h in the dark. After removal of THF under reduced pressure, the aqueous phase was extracted with CH_2Cl_2 (3×). The combined organic phases were dried over Na_2SO_4, and the solvent was removed under reduced pressure. The solid was recrystallized from CH_2Cl_2/acetone (10 mL/5 mL). Filtration of the desired precipitate and washing with CH_2Cl_2 afforded compound **9** as an off-white solid (1.25 g, 2.18 mmol, 70%). Purification of the mother liquor by column chromatography (SiO_2, CH_2Cl_2 → Et_2O) afforded an additional crop of compound **9** (0.44 g, 0.78 mmol, 25%).

^{1}H NMR (400 MHz, $CDCl_3$): δ (ppm) = 8.95 (dd, *J* = 2.4, 0.8 Hz, 1H), 8.75 (dd, *J* = 2.3, 0.9 Hz, 1H), 8.56 – 8.45 (m, 2H), 8.05 (dd, *J* = 8.3, 2.4 Hz, 1H), 7.87 (dd, *J* = 8.2, 2.3 Hz, 1H), 7.69 (d, *J* = 8.1 Hz, 2H), 7.52 (d, *J* = 7.9 Hz, 2H), 7.24 (s, 1H), 7.22 (s, 1H), 7.19 (s, 2H), 5.24 (s, 1H), 4.80 (d, *J* = 4.6 Hz, 2H), 2.35 (s, 3H), 2.34 (s, 3H), 1.79 (t, *J* = 5.4 Hz, 1H), 1.49 (s, 18H).

^{13}C NMR (101 MHz, $CDCl_3$): δ (ppm) = 154.98, 154.27, 153.02, 149.64, 147.76, 142.84, 141.25, 137.73, 137.54, 137.02, 136.38, 136.18, 135.64, 135.29, 133.41, 132.99, 132.48, 132.42, 132.01, 127.87, 127.34, 126.00, 121.13, 120.61, 68.11, 65.05, 34.61, 30.59, 25.75, 20.37, 20.10.

4'-(5'-(4-(Bromomethyl)phenyl)-[2,2'-bipyridin]-5-yl)-3,5-di-tert-butyl-2',5'-dimethyl-[1,1'-biphenyl]-4-ol (10)

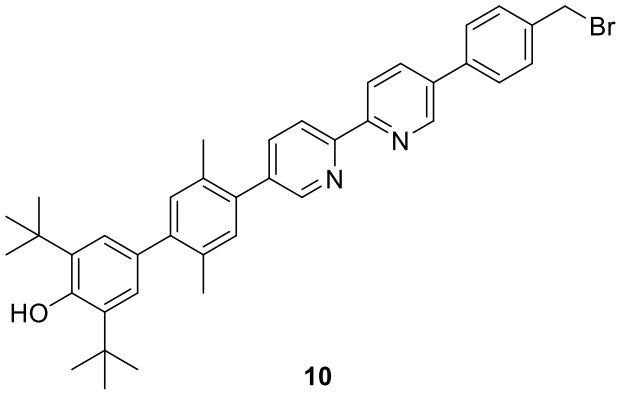

10

PBr_3 (8.32 µL, 87.6 µmol, 1.00 eq.) was added to a suspension of compound **9** (50.0 mg, 87.6 µmol, 1.00 eq.) in dry CH_2Cl_2 (5 mL) at room temperature. The yellow solution was stirred at room temperature for 16 h. Brine was added, and the mixture was stirred for 30 min and subsequently extracted with CH_2Cl_2 (3×). The combined organic phases were dried over Na_2SO_4, and then the solvent was removed under reduced pressure. Purification by column chromatography (SiO_2, Et_2O) afforded compound **10** as an off-white solid (49.4 mg, 78.0 µmol, 89%).

^{1}H NMR (400 MHz, $CDCl_3$): δ (ppm) = 9.02 – 8.88 (m, 1H), 8.75 (dd, *J* = 2.3, 0.8 Hz, 1H), 8.58 – 8.41 (m, 2H), 8.08 – 8.02 (m, 1H), 7.87 (dd, *J* = 8.1, 2.3 Hz, 1H), 7.73 – 7.63 (m, 2H), 7.54 (d, *J* = 8.2 Hz, 2H), 7.24 (s, 1H), 7.21 (s, 1H), 7.19 (s, 2H), 5.24 (s, 1H), 4.62 (d, *J* = 38.0 Hz, 2H), 2.35 (s, 3H), 2.34 (s, 3H), 1.49 (s, 18H).

1-(4-(5'-(3',5'-Di-*tert*-butyl-4'-hydroxy-2,5-dimethyl-[1,1'-biphenyl]-4-yl)-[2,2'-bipyridin]-5-yl)benzyl)-[4,4'-bipyridin]-1-ium bromide (LBr)

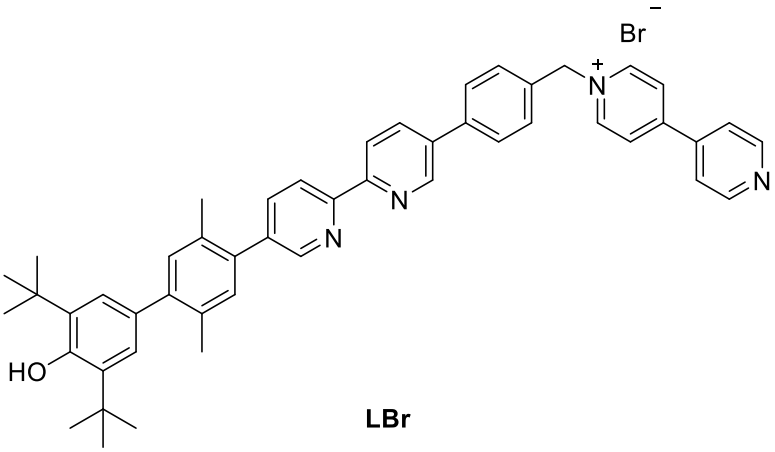

LBr

A solution of compound **10** (159 mg, 251 µmol, 1.00 eq.) and 4,4'-bipyridine (80.0 mg, 512 µmol, 2.04 eq.) in dry CH_2Cl_2 (30 mL) was heated at reflux for 16 h. Then the solvent was removed under reduced pressure. The solid residue was dissolved in $CHCl_3$ (5 mL) and added dropwise to stirring Et_2O. The precipitate was filtered and washed with Et_2O and dried under reduced pressure. The final ligand **LBr** was obtained as an off-white solid (117 mg, 148 µmol, 59 %)
^{1}H NMR (400 MHz, DMSO-d_6): δ (ppm) = 9.61 – 9.18 (m, 2H), 9.10 (s, 1H), 8.94 – 8.84 (m, 2H), 8.77 (s, 1H), 8.71 – 8.66 (m, 2H), 8.55 (s, 2H), 8.34 (s, 1H), 8.07 – 8.03 (m, 2H), 7.99 – 7.95 (m, 2H), 7.78 (d, *J* = 8.0 Hz, 2H), 7.24 (s, 1H), 7.21 (s, 1H), 7.10 (s, 2H), 7.07 (s, 1H), 5.98 (s, 2H), 2.31 (s, 3H), 2.28 (s, 3H), 1.44 (s, 18H).
^{13}C NMR (101 MHz, DMSO-d_6): δ (ppm) = 153.04, 152.91, 150.97, 145.42, 141.02, 138.94, 132.56, 131.99, 131.75, 129.86, 127.70, 126.03, 125.21, 122.11, 62.63, 40.15, 39.94, 39.73, 39.52, 39.31, 39.10, 38.89, 34.64, 30.46, 19.94, 19.64.

$[Ru(bpy)_2(CH_3CN)_2](OTf)_2$ (12)

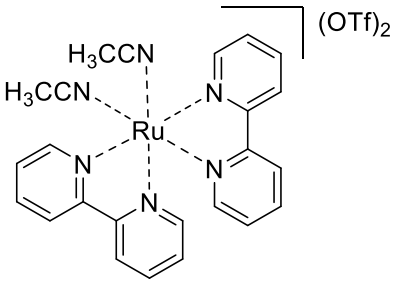

12

A mixture of ruthenium(II) precursor complex **11** (298 mg, 572 µmol, 1.00 eq.) and silver triflate (312 mg, 1.21 mmol, 2.12 eq.) in acetonitrile (100 mL) was degassed and then heated at reflux in the dark for 18 h. After cooling to room temperature, the resulting precipitate was filtered and rinsed with acetonitrile (5 mL). The solvent of the orange filtrate was removed under reduced pressure, and complex **12** was obtained as an orange solid (453 mg, 572 µmol, ~100%)

^{1}H NMR (400 MHz, CD_3CN): δ (ppm) = 9.32 (ddd, *J* = 5.6, 1.5, 0.8 Hz, 2H), 8.52 (dt, *J* = 8.2, 1.0 Hz, 2H), 8.41 – 8.34 (m, 2H), 8.27 (ddd, *J* = 8.2, 7.7, 1.5 Hz, 2H), 7.94 (ddd, *J* = 8.2, 7.6, 1.5 Hz, 2H), 7.85 (ddd, *J* = 7.7, 5.6, 1.3 Hz, 2H), 7.59 (ddd, *J* = 5.7, 1.5, 0.8 Hz, 2H), 7.25 (ddd, *J* = 7.6, 5.7, 1.3 Hz, 2H), 2.27 (s, 6H).

$[Ru(bpy)_2(L)](PF_6)_3$ (PhOH-Ru^{2+}-MQ^+)

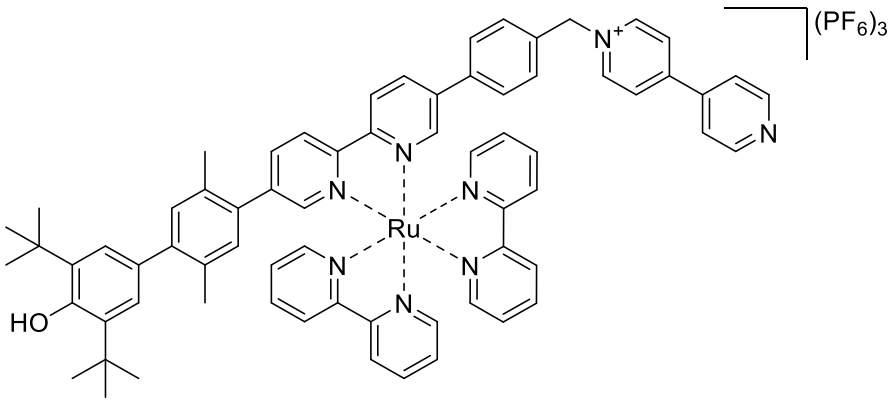

PhOH-Ru^{2+}-MQ^+

A suspension of precursor complex **12** (30.3 mg, 38.0 µmol, 1.00 eq.), the ligand **LBr** (30.0 mg, 38.0 µmol, 1.00 eq.) and silver triflate (15 mg, 58.0 µmol, 1.54 eq.) in ethylene glycol (8 mL) was degassed and then heated at 105 °C for 4 d. After cooling to room temperature, the mixture was taken up in methanol and acetone and filtered through a pad of celite, which was then rinsed with acetone. The solvent was removed under reduced pressure, and the residue was purified by column chromatography (SiO_2, acetone → acetone, water, saturated aqueous KNO_3 100:10:1 → acetone, water, saturated aqueous KNO_3 100:50:10). Acetate buffer (pH 5, 0.1 M, 10 mL) and saturated aqueous KPF_6 solution were added to the last red fraction which contained the desired triad. The organic solvent was removed under reduced pressure. The resulting precipitate was filtered, washed with water and dried under reduced pressure. **$[Ru(bpy)_2(L)](PF_6)_3$ (PhOH-Ru^{2+}-MQ^+)** was obtained as a red solid (53 mg, 34 µmol, 90%).

^{1}H NMR (400 MHz, CD_3CN): δ (ppm) = 8.90 – 8.80 (m, 4H), 8.65 – 8.56 (m, 2H), 8.53 – 8.47 (m, 3H), 8.37 – 8.30 (m, 3H), 8.16 – 7.99 (m, 6H), 7.93 – 7.87 (m, 2H), 7.84 (dd, *J* = 2.0, 0.7 Hz, 1H), 7.82 (ddd, *J* = 5.6, 1.6, 0.7 Hz, 1H), 7.80 – 7.77 (m, 2H), 7.73 (ddd, *J* = 5.6, 1.5, 0.7 Hz, 1H), 7.63 (dd, *J* = 2.0, 0.7 Hz, 1H), 7.51 (d, *J* = 0.8 Hz, 4H), 7.48 – 7.34 (m, 4H), 7.12 (s, 1H), 7.10 (s, 2H), 7.05 (s, 1H), 5.77 (s, 2H), 5.57 (s, 1H), 2.23 (s, 3H), 1.98 (s, 3H), 1.43 (s, 18H).

HRMS: $[M]^{3+}$ calculated (*m*/*z*) for $C_{69}H_{65}N_8ORu$: 374.4776, found: 374.4782.

Anal. Calcd. for $C_{69}H_{65}F_{18}N_8OP_3Ru \cdot 0.4\ C_3H_6O \cdot 2.5\ H_2O$: C 51.84, H 4.49, N 6.89; found: C 51.53, H 4.87, N 7.27.

(4-([2,2'-Bipyridin]-5-yl)phenyl)methanol (14)

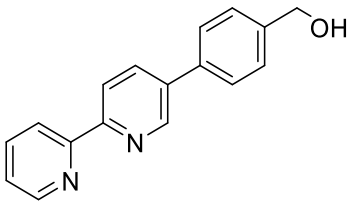

14

A mixture of **13** (502 mg, 2.10 mmol, 1.00 eq.), 4-(hydroxymethyl)phenylboronic acid (380 mg, 2.50 mmol, 1.20 eq.), K_2CO_3 (806 mg, 6.30 mmol, 3.00 eq.), THF (18 mL) and water (3 mL) was degassed. After addition of $Pd(PPh_3)_4$ (218 mg, 311 µmol, 14.8 mol%) the mixture was degassed again and heated at reflux for 48 h. After cooling to room temperature, the mixture was extracted with CH_2Cl_2 (3×), the combined organic phases were dried over Na_2SO_4, and the solvent was removed under reduced pressure. Purification by column chromatography (SiO_2, pentane/ethyl acetate 8:1→ 5:1) afforded compound **14** as a white solid (390 mg, 1.50 mmol, 71%).

^{1}H NMR (400 MHz, $CDCl_3$): δ (ppm) = 8.92 (d, *J* = 2.4 Hz, 1H), 8.71 (ddd, *J* = 4.8, 1.9, 0.9 Hz, 1H), 8.48 (d, *J* = 8.2 Hz, 1H), 8.45 (d, *J* = 7.9 Hz, 1H), 8.03 (dd, *J* = 8.3, 2.4 Hz, 1H), 7.85 (dd, *J* = 7.7, 1.8 Hz, 1H), 7.67 (m, 2H), 7.52 (m, 1H), 7.34 (ddd, *J* = 7.5, 4.8, 1.2 Hz, 1H), 4.78 (s, 2H), 1.83 (1H).

5-(4-(Bromomethyl)phenyl)-2,2'-bipyridine (15)

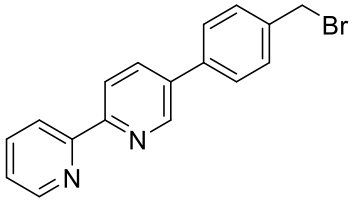

15

At room temperature, PBr_3 (25.4 µL, 266 µmol, 1.00 eq.) was added to a solution of compound **14** (70.0 mg, 266 µmol, 1.00 eq.) in dry CH_2Cl_2 (5 mL). The yellow solution was stirred at room temperature for 16 h. Brine was added, the mixture was stirred for 30 min and then extracted with CH_2Cl_2 (3×). The combined organic phases were dried over Na_2SO_4, and the solvent was removed under reduced pressure. Purification by column chromatography (SiO_2, Et_2O) afforded compound **15** as a white solid (45 mg, 138 µmol, 52%).

^{1}H NMR (400 MHz, $CDCl_3$): δ (ppm) = 9.93 (dd, *J* = 2.5, 0.9 Hz, 1H), 8.72 (dd, *J* = 5.0, 1.9 Hz, 1H), 8.53 (s, 2H), 8.04 (dd, *J* = 8.3, 2.3 Hz, 1H), 7.87 (td, *J* = 7.8, 1.8 Hz, 1H), 7.64 (d, *J* = 8.2 Hz, 2H), 7.54 (d, *J* = 8.2 Hz, 2H), 7.36 (ddd, *J* = 7.5, 4.8, 1.2 Hz, 1H), 4.57 (s, 2H).

1-(4-([2,2'-Bipyridin]-5-yl)benzyl)-[4,4'-bipyridin]-1-ium bromide ($L^{MQ}Br$)

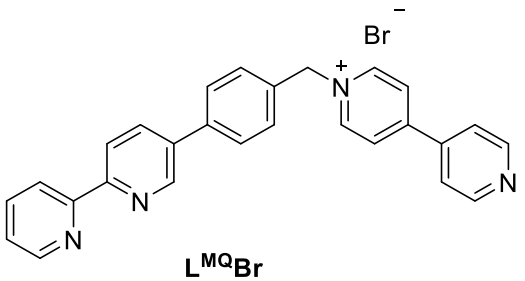

$L^{MQ}Br$

A solution of compound **15** (40.0 mg, 123 µmol, 1.00 eq.) and 4,4'-bipyridine (96.0 mg, 615 µmol, 5,0 eq.) in dry CH_2Cl_2 (10 mL) was heated at reflux for 16 h. The white precipitate was filtered and washed with CH_2Cl_2. The white solid was collected from the frit with a mixture of $CHCl_3$ and methanol (100:1). Evaporation of the solvent yielded **$L^{MQ}Br$** as a white solid (58.5 mg, 122 µmol, 99%).

^{1}H NMR (400 MHz, $CD_3OD/CDCl_3$ 15:10): δ (ppm) = 9.27 (d, *J* = 6.9 Hz, 2H), 8.86 (d, *J* = 1.9 Hz, 1H), 8.78 – 8.71 (m, 2H), 8.64 (d, *J* = 4.7 Hz, 1H), 8.41 (d, *J* = 7.1 Hz, 2H), 8.34 (dd, *J* = 7.9, 2.5 Hz, 2H), 8.10 (dd, *J* = 8.3, 2.4 Hz, 1H), 8.00 (td, *J* = 7.8, 1.8 Hz, 1H), 7.84 – 7.79 (m, 2H), 7.76 – 7.67 (m, 4H), 7.48 (ddd, *J* = 7.5, 5.0, 1.2 Hz, 1H), 5.97 (s, 2H).

^{13}C NMR (101 MHz, $CD_3OD/CDCl_3$ 15:10): δ (ppm) = 155.55, 154.99, 154.39, 152.06, 149.30, 148.66, 146.77, 143.23, 140.83, 140.06, 137.72, 137.66, 134.42, 131.63, 129.76, 127.66, 126.28, 123.60, 123.57, 123.33, 65.29.

$[Ru(bpy)_2(L^{MQ})](PF_6)_3$ (Ru^{2+}-MQ^+ reference dyad**)**

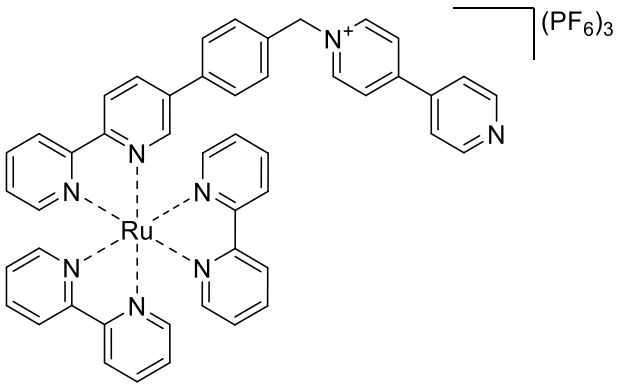

Ru^{2+}-MQ^+

A suspension of precursor complex **12** (74.2 mg, 93.5 µmol, 1.02 eq.), the ligand **$L^{MQ}Br$** (44.0 mg, 91.4 µmol, 1.00 eq.) and silver triflate (40.0 mg, 156 µmol, 1.70 eq.) in ethylene glycol (10 mL) was degassed and then heated at 105 °C for 4 d. After cooling to room temperature, the mixture was taken up in methanol and acetone and filtered through a pad of celite, which was then rinsed with acetone. The solvent was removed under reduced pressure and the residue was purified by column chromatography (SiO_2, acetone → acetone, water, saturated aqueous KNO_3 100:10:1 → acetone, water, saturated aqueous KNO_3 100:50:10). Saturated aqueous KPF_6 solution was added to the second red-colored fraction which contained the desired triad. The organic solvent was removed under reduced pressure. The resulting precipitate was filtered, washed with cold water and Et_2O. The red solid was taken up in CH_2Cl_2 (50 mL) and the organic phase was washed with water containing 10% acetate buffer (pH 5, 0.1 M, 10 mL) (3×50 mL). The combined aqueous phases were extracted with CH_2Cl_2 (1×10 mL). To the combined aqueous phases was added saturated aqueous KPF_6

solution and the mixture was stored for 0.5 h at 5 °C. Filtration and washing with cold water (30 mL) and Et_2O (30 mL) yielded a red solid, that was collected from the frit with acetone and subjected to column chromatography (SiO_2, acetone → acetone, water, saturated aqueous KNO_3 100:10:1 → acetone, water, saturated aqueous KNO_3 100:50:10). Saturated aqueous KPF_6 solution and acetate buffer (pH 5, 0.1 M) was added to the second red fraction which contained the desired triad. The organic solvent was removed under reduced pressure. The resulting precipitate was filtered, washed with cold water and Et_2O. The red solid was collected from the frit with acetone. Solvent removal under reduced pressure yielded **$[Ru(bpy)_2(L^{MQ})](PF_6)_3$ (Ru^{2+}-MQ^+)** as a red solid (46 mg, 37 µmol, 40%).

^{1}H NMR (400 MHz, CD_3CN): δ (ppm) = 8.87 – 8.84 (m, 2H), 8.83 – 8.79 (m, 2H), 8.56 (d, *J* = 8.0 Hz, 1H), 8.53 (dt, *J* = 8.3, 1.1 Hz, 1H), 8.49 (d, *J* = 8.6 Hz, 4H), 8.33 (d, *J* = 6.7 Hz, 2H), 8.29 (dd, *J* = 8.5, 2.1 Hz, 1H), 8.11 – 7.99 (m, 5H), 7.84 (ddd, *J* = 5.7, 1.5, 0.7 Hz, 1H), 7.81 (dd, *J* = 2.1, 0.7 Hz, 1H), 7.80 – 7.76 (m, 3H), 7.76 – 7.72 (m, 2H), 7.70 (ddd, *J* = 5.7, 1.5, 0.7 Hz, 1H), 7.49 (s, 4H), 7.44 – 7.34 (m, 5H), 5.75 (s, 2H).

HRMS: $[M]^{3+}$ calculated (*m*/*z*) for $C_{47}H_{37}N_8ORu$: 271.7393, found: 271.7394.

Anal. Calcd. for $C_{47}H_{37}F_{18}N_8OP_3Ru \cdot 0.65\ C_3H_6O \cdot 2.8\ H_2O$: C 43.94, H 3.50, N 8.37; found: C 43.76, H 3.69, N 8.56.

[1]H NMR spectra of the triad and the reference dyad

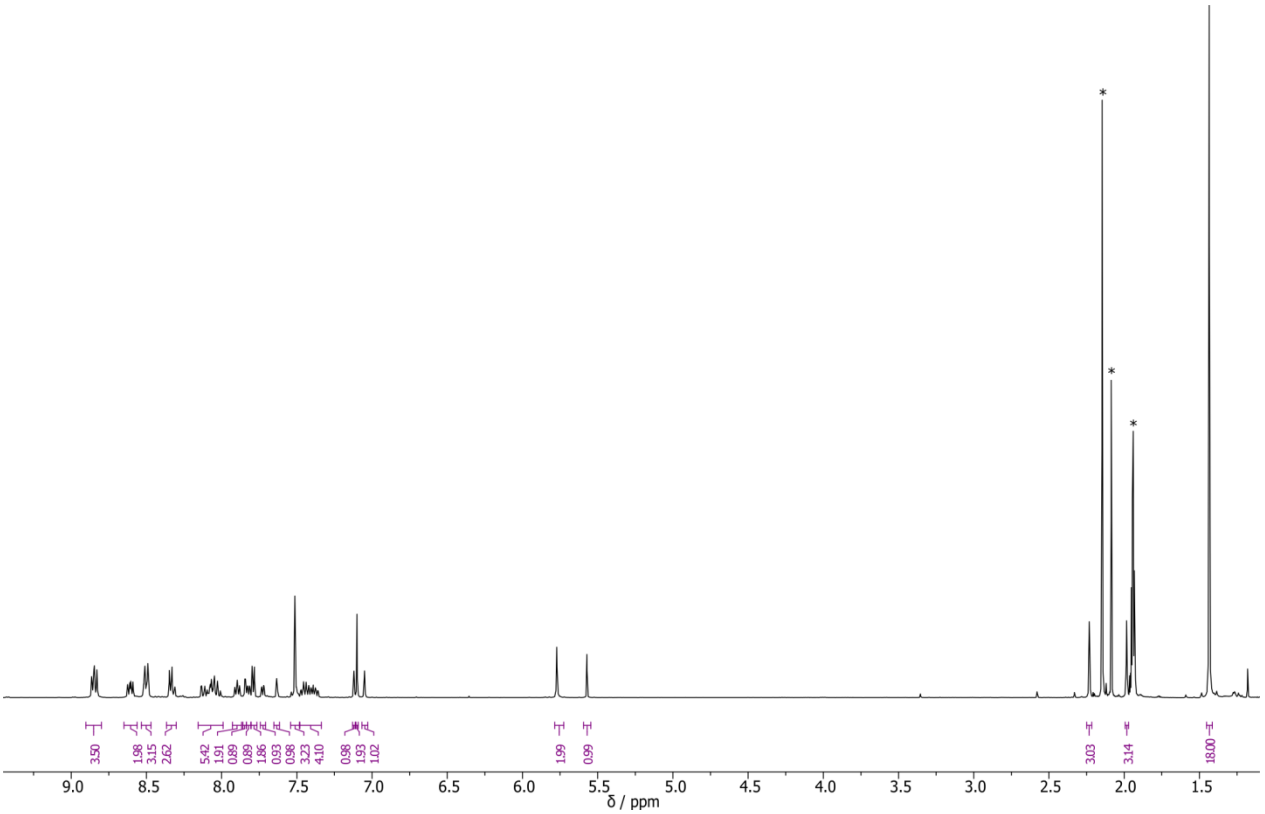

Figure S1. [1]H NMR spectrum of the PhOH-Ru(II)-MQ^+ triad in CD_3CN. Resonances from the solvents water and acetone, and the residual solvent peak of CD_3CN are marked with an asterisk (*).

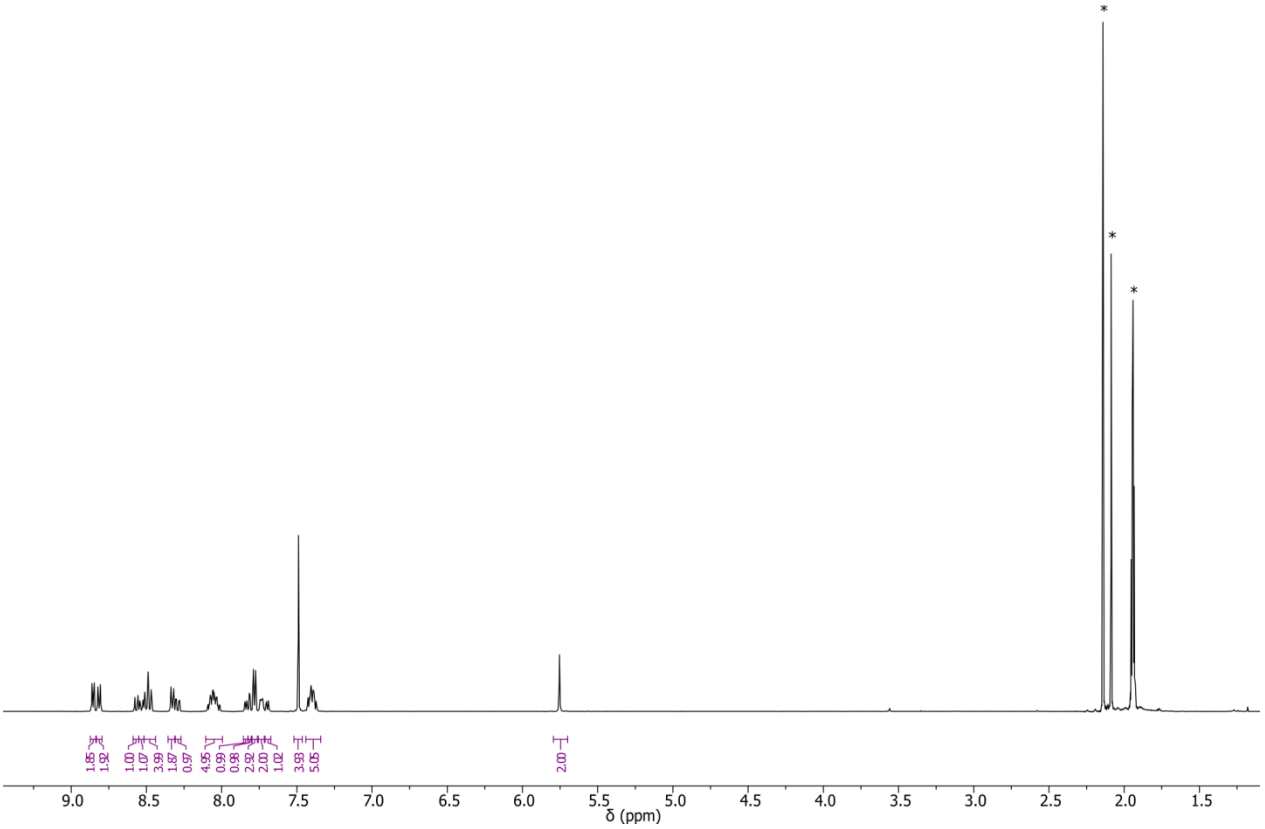

Figure S2. [1]H NMR spectrum of the Ru(II)-MQ^+ dyad in CD_3CN. Resonances from the solvents water and acetone, and the residual solvent peak of CD_3CN are marked with an asterisk (*).

Equipment and methods

All commercially available chemicals for synthesis were used as received. NMR spectroscopy was performed using a Bruker Avance III instrument operating at 400 MHz frequency for ^{1}H and at 101 MHz for ^{13}C. The instrument was equipped with a direct observe 5-mm BBFO smart probe and the solvent residual peak was used as internal reference. High resolution mass spectra were measured on a Bruker maXis 4G QTOF spectrometer. Elemental analyses were conducted on a Vario Micro Cube instrument from Elementar by Ms. Sylvie Mittelheisser in the Department of Chemistry at University of Basel.

Acetonitrile and pyridine for electrochemical and photophysical measurements was HPLC grade or higher. Mixtures of pyridine with pyridinium were prepared by carefully adding triflic acid to the pyridine solution. Electrochemical measurements took place at 22 °C and photophysical measurements were performed at 25 °C. Steady-state luminescence experiments were performed on a Fluorolog-3 apparatus from Horiba Jobin-Yvon. Luminescence lifetime and transient absorption experiments occurred on an LP920-KS spectrometer from Edinburgh Instruments equipped with an iCCD detector from Andor. The excitation source was the frequency-doubled output from a Quantel Brilliant b laser. For all de-aerated optical spectroscopic experiments, the samples were de-oxygenated via two subsequent freeze–pump–thaw cycles in quartz cuvettes that were specifically designed for this purpose. UV-Vis spectra were measured on a Cary 5000 instrument from Varian. Cyclic voltammetry was performed on a Versastat3-200 potentiostat from Princeton Applied Research using a glassy carbon disk working electrode, a saturated calomel electrode (SCE) as reference electrode, and a platinum wire as counter electrode. For cyclic voltammetry in CH_3CN and in neat pyridine, 0.1 M $TBAPF_6$ served as electrolyte. In pyridine / 0.22 M pyridinium solution no additional supporting electrolyte was added. Prior to voltage sweeps at rates of 0.1 V s^{-1}, the solutions were flushed with argon. For quasi-reversible cyclic voltammograms the average of reductive and oxidative peak potential was used to determine the redox potential, for irreversible processes the inflection point of the voltage curve is reported. UV-vis spectra of electrochemically generated species were recorded with the Cary 5000 instrument by applying voltage with a Versastat3-200 potentiostat, using a platinum gauze electrode as working electrode, a saturated calomel electrode (SCE) as reference electrode, and a platinum wire as counter electrode. The substance was dissolved in CH_3CN with 0.1 M $TBAPF_6$ as supporting electrolyte and the suitable potential was applied in a spectroelectrochemical cell from *ALS* with 1 mm path length. Potentials for electrolysis were determined by cyclic voltammetry. The following experimental uncertainties were taken into account: Excited state lifetimes were considered accurate to 10%, and ground state redox potentials are considered accurate to ±0.05 V.

Optical spectroscopy of the triad in CH_3CN

Excitation of the PhOH-Ru(II)-MQ^+ triad in de-aerated CH_3CN at 532 nm with laser pulses of ~10 ns duration yields the spectrum shown in **Figure S3**. The signal was time-integrated over a period of 200 ns immediately after excitation.

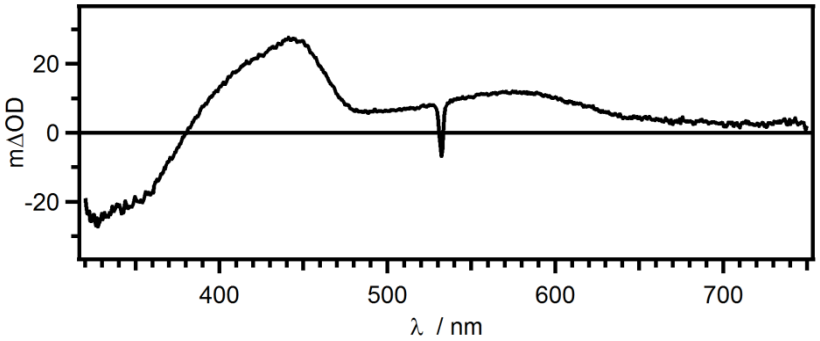

Figure S3. Transient absorption spectrum of 27 μM triad in neat, de-aerated CH_3CN, recorded directly after excitation at 532 nm with laser pulses of ~10 ns duration.

Under comparable conditions steady-state irradiation at 450 nm of the triad yields the luminescence spectrum shown in **Figure S4**.

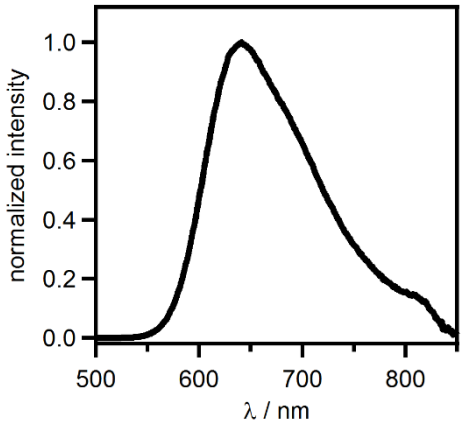

Figure S4. Luminescence spectrum of 23 μM triad in CH_3CN after excitation at 450 nm.

The luminescence band in **Figure S4** is compatible with ^{3}MLCT emission from the Ru(II) photosensitizer. After pulsed excitation, the luminescence intensity at 630 nm decays with the same time constant (τ = 800±80 ns) as the transient absorption signals at 445 and 570 nm (**Figure S5**). Thus, no photochemistry occurs after excitation of the triad in neat CH_3CN, and there is merely ^{3}MLCT photoluminescence. The transient absorption spectrum in **Figure S3** is the signature of that ^{3}MLCT state.[7,8]

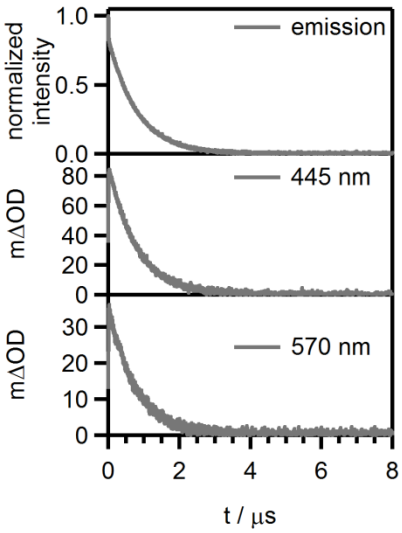

Figure S5. Kinetic data for 35 μM triad in neat, de-aerated CH_3CN after excitation at 532 nm with pulses of ~10 ns duration: Decay of the luminescence intensity at 630 nm (top), and decay of the transient absorption signals at 445 nm (middle) and 570 nm (bottom).

Acid-base equilibrium between phenol and pyridine

The UV-Vis absorption spectra of the triad in CH_3CN and in pyridine are very similar (black and green traces in **Figure S6**). This indicates that the phenolic unit of the triad remains largely protonated in neat pyridine.

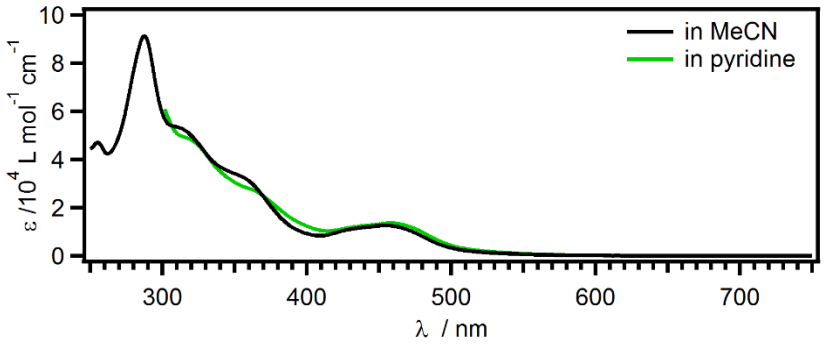

Figure S6. Optical absorption spectra of the triad in CH_3CN (black trace) and in pyridine (green trace). At wavelengths shorter than 300 nm, pyridine is not sufficiently transparent hence the respective spectrum is cut at this wavelength.

The phenolic unit of the PhOH-Ru(II)-MQ^+ triad in pyridine is in an acid-base equilibrium with the solvent:

$$PhOH + py \leftrightarrows PhO^- + pyH^+ \qquad \text{(eq. S1)}$$

The law of mass action for this reaction is:

$$K = \frac{[pyH^+]\cdot[PhO^-]}{[PhOH]\cdot[py]} \qquad \text{(eq. S2)}$$

The equilibrium constant K can be calculated from the acidity constants of PhOH (pK_{a1}) and pyH^+ (pK_{a2}) according to eq. S3. We use the following values for CH_3CN solution: $pK_{a1} = 28$,[9] $pK_{a2} = 12.5$.[10]

$$K = 10^{-\Delta pKa} = 10^{-(pKa1-pKa2)} = 10^{-(28-12.5)} = 10^{-15.5} \qquad \text{(eq. S3)}$$

With $[pyH^+] = [PhO^-]$, eq. S2 simplifies to:

$$([PhOH])^2 = K\cdot[py]\cdot[PhOH] \qquad \text{(eq. S4)}$$

Using $K = 10^{-15.5}$ (from eq. S3), [py] = 12.4 M (the molarity of neat pyridine), and $[PhOH] = 3\cdot10^{-5}$ M (a typical triad concentration used in our experiments), one obtains $[PhO^-] = 3.4\cdot10^{-10}$ M. This suggests that in a pyridine solution containing $3\cdot10^{-5}$ M triad only $\sim10^{-3}$ % of the phenolic units are deprotonated. This analysis is a rather crude approximation, because it relies on acidity constants for CH_3CN, applied to a situation in which pyridine is effectively the solvent.

Nevertheless, ^{1}H NMR experiments of the phenol in pyridine support the view that only a very small fraction of phenolic units is deprotonated by pyridine yielding pyridinium. In neat C_5D_5N the phenolic O-H resonance is clearly visible at 7.97 ppm, whereas the N-H resonance of pyridinium in that solvent is at 14.6 ppm (**Figure S7**).

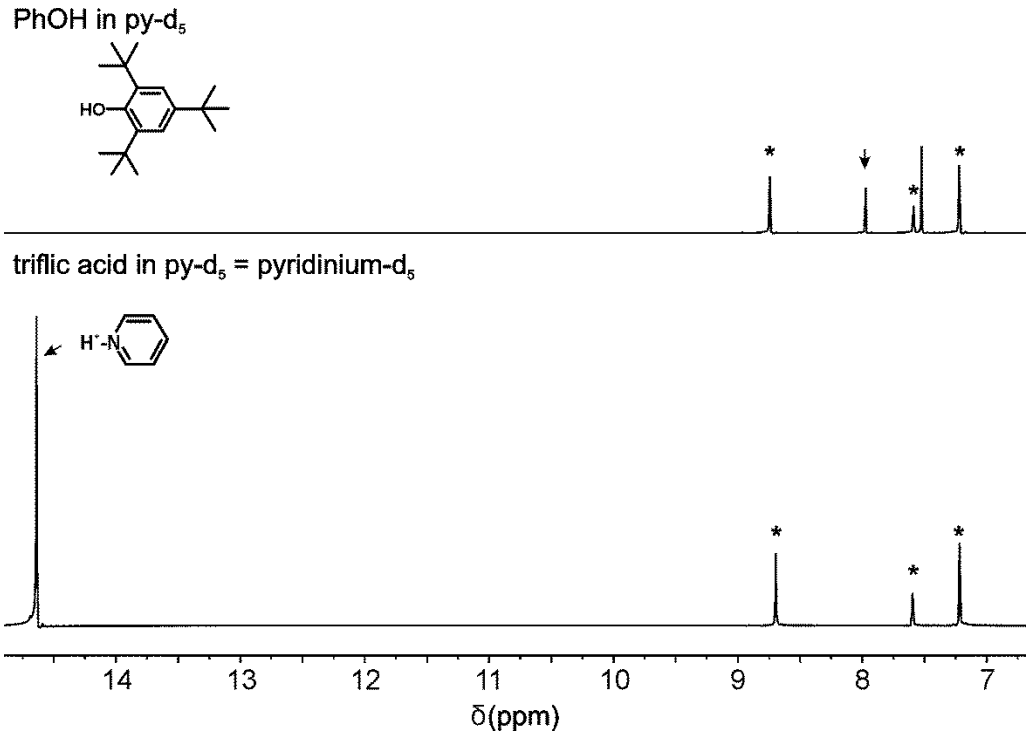

Figure S7. ^{1}H NMR spectrum of 2,4,6-tri-*tert*-butylphenol in neat pyridine-d_5 (top) and ^{1}H NMR spectrum of pyridinium-d_5 generated by addition of 0.21 M triflic acid to pyridine-d_5 (bottom). Signals marked with asterisks are due to residual non-deuterated pyridine. The phenolic proton and the pyridinium-N-H resonance are marked by arrows.

Hydrogen-bonding equilibrium between phenol and pyridine

In neat CD_3CN, the resonance of the phenolic proton of 2,4,6-tri-*tert*-butylphenol is observed at 5.26 ppm. Upon addition of increasing amounts of pyridine, this resonance shifts to lower fields, and finally after addition of 100 equivalents of pyridine, the phenolic resonance appears at 6.04 ppm (**Figure S8**). In neat C_5D_5N, the phenolic resonance is still clearly visible at 7.97 ppm, consistent with our conclusion on pages S17/18 that the phenolic proton is hydrogen-bonding to pyridine rather than being deprotonated in substantial amounts. As noted above (**Figure S7**), the pyridinium N-H resonance in pyridine-d_5 appears at 14.6 ppm. This signal is not observable in any of the spectra from **Figure S8**.

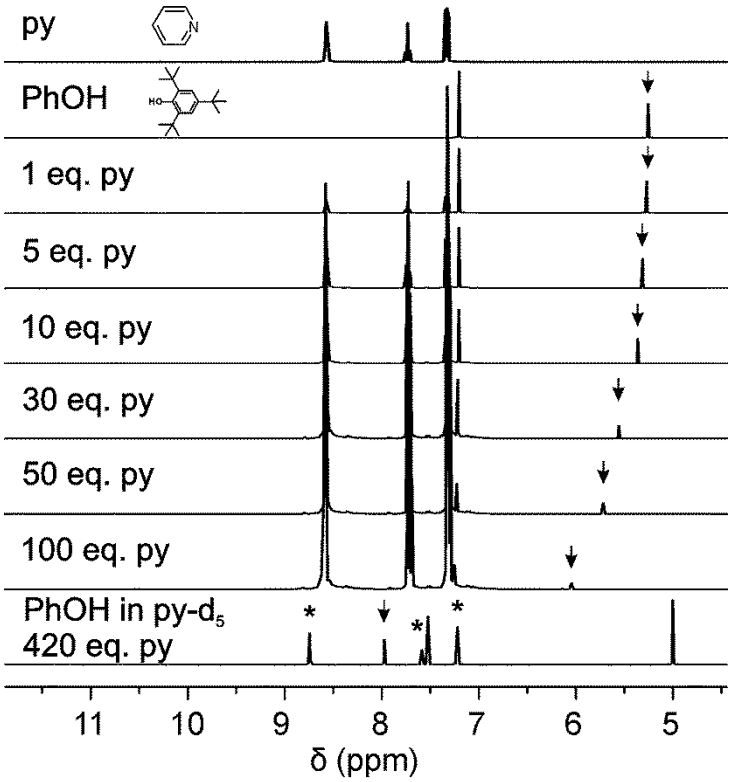

Figure S8. ^{1}H NMR spectra of 2,4,6-tri-*tert*-butylphenol in neat CD_3CN and in presence of various amounts of pyridine. The ^{1}H NMR spectrum of pyridine is shown at the top. The bottom spectrum was recorded in neat pyridine-d_5 (equals 420 eq. pyridine); signals marked with asterisks are due to residual non-deuterated pyridine. The phenolic proton resonance is marked by an arrow in all spectra.

The change in chemical shift of the phenolic resonance signal as a function of pyridine concentration is attributed to hydrogen-bonding, as observed in phenols previously.[11] **Figure S9** contains a plot of these data that can be used for the determination of the association constant $K_{H\text{-}bond}$ describing the hydrogen-bonding interaction between the phenolic unit and pyridine (eqs. S5, S6).

$$\mathrm{PhOH} + \mathrm{py} \leftrightarrows \mathrm{PhOH\cdots py} \qquad \text{(eq. S5)}$$

$$K_{H\text{-}bond} = \frac{[\mathrm{PhOH\cdots py}]}{[\mathrm{PhOH}]\cdot[\mathrm{py}]} \qquad \text{(eq. S6)}$$

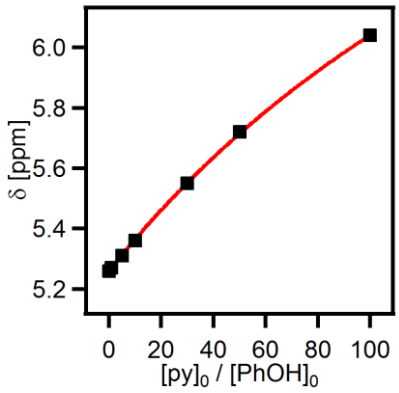

Figure S9. Chemical shift of the ^{1}H NMR resonance for the phenolic proton of 2,4,6-tri-*tert*-butylphenol in the titrations from **Figure S8**. The solid red line represents the best fit to the experimental data (black squares) according to equations S7-S9 in order to determine $K_{H\text{-}bond}$.

The association constant $K_{H\text{-}bond}$ was determined with a two-parameter fit suitable for fast exchange conditions (eq. S7, S8).[12] Apart from $K_{H\text{-}bond}$, the second unknown is the chemical shift of the phenol OH resonance in the limit when all phenol molecules present in solution are hydrogen-bonded to pyridine ($\delta_{PhOH\cdots py}$) (eq. S9). δ is the experimentally observable chemical shift at a given pyridine concentration. $[py]_0$ and $[PhOH]_0$ are the nominal pyridine and phenol concentrations, respectively.

$$\delta = \delta_{PhOH} - \left(\frac{\Delta\delta}{2}\right) \cdot \left(b - \sqrt{b^2 - 4\left(\frac{[py]_0}{[PhOH]_0}\right)}\right) \qquad \text{(eq. S7)}$$

$$b = 1 + \frac{[py]_0}{[PhOH]_0} + \frac{1}{(K_{H\text{-}bond} \cdot [PhOH]_0)} \qquad \text{(eq. S8)}$$

$$\Delta\delta = \delta_{PhOH} - \delta_{PhOH\cdots py} \qquad \text{(eq. S9)}$$

The outcome of this analysis is that $K_{H\text{-}bond} \approx 0.16 \pm 0.04$ M^{-1}. Thus, hydrogen-bonding between the phenolic unit of the triad and pyridine is very weak, presumably due to the sterically demanding *tert*-butyl substituents in *ortho*-position to the hydroxyl group.

Phenols without *ortho*-substituents have association constants about an order of magnitude larger in CD_3CN and in benzonitrile.[11,13]

The fit further yielded $\delta_{PhOH\cdots py} = 8.0 \pm 0.1$ ppm for the chemical shift in the limit in which all phenol molecules are hydrogen-bonded, compatible with the observable chemical shift in pyridine-d_5 (7.97 ppm, see above).

Using eq. S6 with $K_{H\text{-}bond} \approx 0.16$ M^{-1} and [py] = 12.5 M, the ratio $\frac{[PhOH\cdots py]}{[PhOH]}$ in pyridine solution is approximately $\frac{2}{1}$.

We note that some of the evidence discussed in the main paper suggests that not all triad molecules are hydrogen-bonded, even in neat pyridine.

Electrochemistry and spectro-electrochemistry of the monoquat unit in CH_3CN

The cyclic voltammogram of *N*-methyl-4,4'-bipyridinium (MQ^+) was recorded in CH_3CN containing 0.1 M $TBAPF_6$ (tetra-*n*-butylammonium hexafluorophosphate) as a supporting electrolyte. Two quasi-reversible reduction waves are observed (**Figure S10a**), in line with prior reports.[6,14,15]

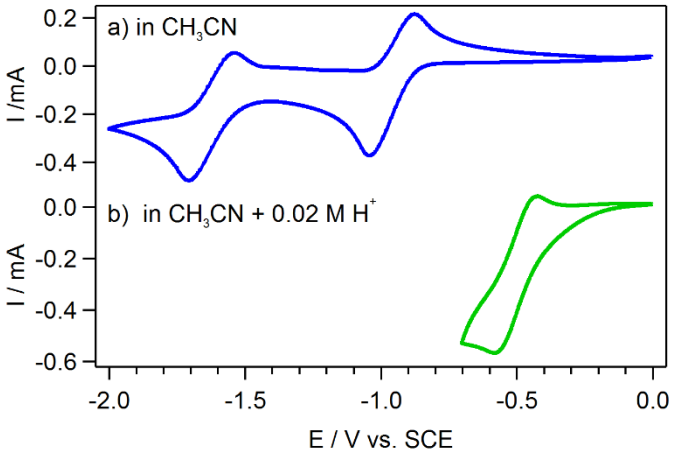

Figure S10. (a) Cyclic voltammogram of 0.02 M MQ^+ in CH_3CN; (b) cyclic voltammogram of 0.01 M MQ^+ in CH_3CN with 0.02 M triflic acid. The supporting electrolyte was 0.1 M $TBAPF_6$ in both cases, and the potential sweep rate was 0.1 V s^{-1}.

In presence of 0.02 M triflic acid, only the first reduction wave of 0.01 M MQ^+ was quasi-reversible (**Figure S10b**). This wave corresponds to the reduction of protonated monoquat (MQH^{2+}), and the determined reduction potential of this compound is in line with that of methyl viologen.[14,15] **Table S1** summarizes the monoquat reduction potentials in CH_3CN.

Table S1. Reduction potentials (E^0) of MQ^+ and MQH^{2+} in CH_3CN. $E_{p,a}$-$E_{p,c}$ is the difference between anodic and cathodic peak currents.

redox couple	E^0 [V vs. SCE]	$E_{p,a}$-$E_{p,c}$ [mV]
$MQ^{+/\bullet}$	-0.96±0.05	170
$MQ^{\bullet/-}$	-1.62±0.05	170
$MQH^{2+/\bullet+}$	-0.50±0.05	160

The spectro-electrochemical trace of $MQ^{\bullet}$ in Figure 2b of the main paper was obtained by applying a potential of -1.0 V vs. SCE to a 0.02 M solution of $MQPF_6$ in de-aerated CH_3CN containing 0.1 M $TBAPF_6$. The spectro-electrochemical trace of $MQH^{\bullet+}$ in Figure 2b of the main paper was recorded while applying a potential of -0.5 V vs. SCE to a 0.01 M solution of $MQPF_6$ in de-aerated CH_3CN containing 0.02 M triflic acid and 0.1 M $TBAPF_6$.

The extinction coefficients were estimated from comparison with previously published spectra.[14]

Electrochemistry of the phenolic unit and UV-Vis spectrum of the phenoxyl radical

The cyclic voltammogram of 2,4,6-tri-*tert*-butylphenol in CH_3CN with 0.1 M $TBAPF_6$ is shown in **Figure S11**. From the inflection point in the irreversible oxidation wave, one estimates an oxidation potential of 1.40 V vs. SCE, in line with prior reports.[9]

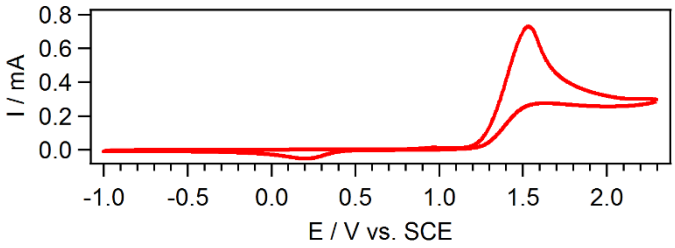

Figure S11. Cyclic voltammogram of 2,4,6-tri-*tert*-butylphenol in CH_3CN with 0.1 M $TBAPF_6$ as supporting electrolyte at a scan rate of 0.1 V s^{-1}.

In order to obtain a reference UV-Vis spectrum of the neutral phenoxyl radical that was expected to form as a photoproduct in the triad, a phenol reference compound that has an attached *p*-xylene moiety was needed. Compound **4** (page S3) was useful for this purpose. The respective compound was converted to its phenoxyl radical form in a 1:6 (v:v) mixture of pyridine and toluene using an aqueous solution of $K_3[Fe(CN)_6]$ in 0.05 M NaOH as an oxidant following a published procedure.[16] The result is shown in Figure 2c of the main paper, and the respective spectrum is in line with previously published UV-Vis spectra of related phenoxyl radicals.[17–19]

The extinction coefficients were estimated by comparison with previously published spectra of phenoxyl radicals.[16,18]

Electrochemistry of the triad in CH_3CN

The cyclic voltammogram of the triad in CH_3CN is shown in **Figure S12** (green trace) along with the cyclic voltammograms of $Ru(bpy)_3^{2+}$ (black trace), the MQ^+ reference compound (blue trace; from **Figure S10**), and 2,4,6-tri-*tert*-butylphenol (red trace; from **Figure S11**). This comparison facilitates attribution of the individual waves to different redox processes expected for the triad.

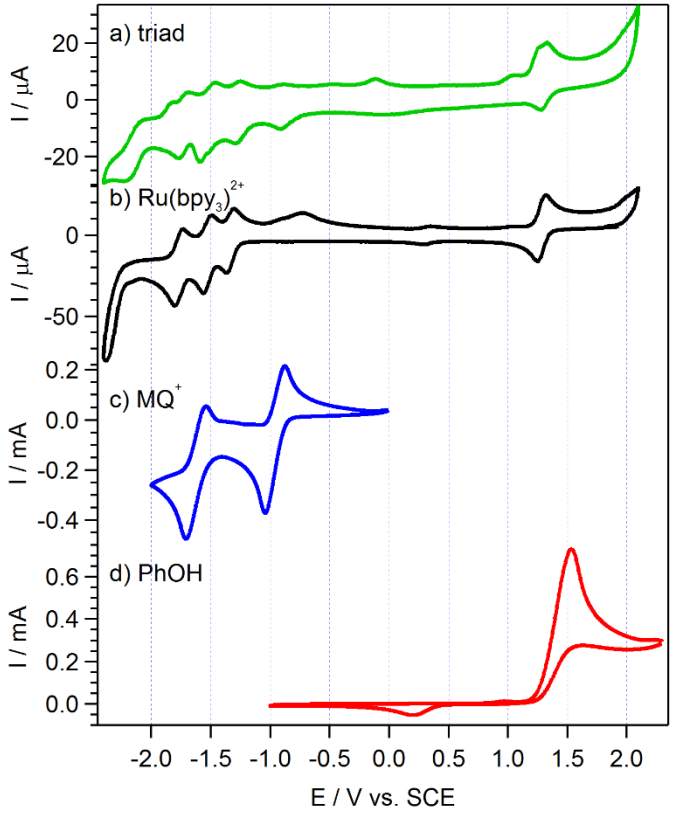

Figure S12. Cyclic voltammograms in CH_3CN with 0.1 M $TBAPF_6$ recorded at potential sweep rates of 0.1 V s^{-1}.

In the oxidative sweep of the triad, one detects two overlapping waves that can be attributed to oxidation of the phenolic unit to the phenoxyl radical cation and to oxidation of Ru(II) to Ru(III). In the reductive sweep one readily recognizes the first MQ^+ reduction while the second reduction of this moiety overlaps with the reduction of one of the three bpy ligands.

The wave at -0.16 V vs. SCE is attributed to oxidation of the phenolate species (PhO^-) to phenoxyl radical ($PhO^•$). PhO^- forms after initial oxidation of PhOH at 1.25 V vs. SCE. The resulting $PhOH^+$ species is highly acidic and releases a proton to the electrolyte solution, and the resulting phenoxyl radical is reduced to phenolate in the subsequent reductive sweep. Upon increasing the potential again, phenolate oxidation then occurs at -0.16 V vs. SCE, in line with prior studies.[1]

The redox potentials extracted from this data are summarized in **Table S2**.

Table S2. Redox potentials of the individual components of the triad in CH_3CN (in V vs. SCE), determined from the data in **Figure S12**.

redox couple	triad	$Ru(bpy)_3^{2+}$ [a]	2,4,6-^{tBu}PhOH [b]	MQ^+ [c]
Ru(III/II)	1.30	1.28		
$PhOH^{\bullet+/0}$	1.25		1.40	
$PhO^{\bullet/-}$	-0.12		-0.32	
$MQ^{+/\bullet}$	-0.89			-0.96
$MQH^{2+/\bullet+}$				-0.50
$MQ^{\bullet/-}$	-1.66			-1.62
$bpy^{0/-}$	-1.26	-1.33		
$bpy^{0/-}$	-1.49	-1.53		
$bpy^{0/-}$	-1.81	-1.77		

[a] Measured on $[Ru(bpy)_3](PF_6)_2$ in CH_3CN. [b] From ref. [9]. [c] Measured on the monoquat reference compound shown in Figure 2b of the main paper. Ground state redox potentials are considered accurate to ±0.05 V.

Electrochemistry in pyridine

The cyclic voltammogram of $[Ru(bpy)_3](PF_6)_2$ in pyridine is shown in **Figure S13**. Reduction and oxidation waves are slightly shifted compared to CH_3CN solution.[20] In pyridine, the first reduction takes place at -1.22±0.05 V vs. SCE, whereas and the $Ru^{II/III}$ oxidation is at 1.40±0.05 V vs. SCE and is irreversible on the time scale of this cyclic voltammogram experiment.

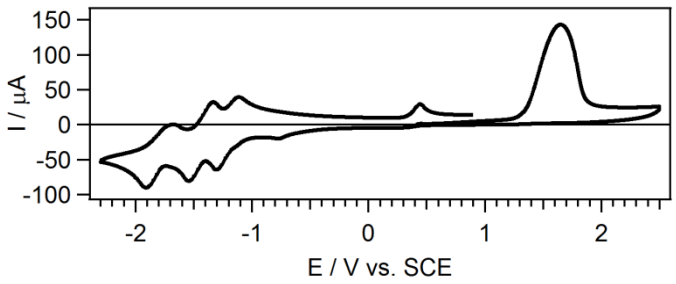

Figure S13. Cyclic voltammogram of $[Ru(bpy)_3](PF_6)_2$ in pyridine with 0.1 M $TBAPF_6$ recorded at potential sweep rates of 0.1 V s^{-1}.

In order to assess the PCET thermodynamics of the MQ^+ acceptor unit, cyclic voltammetry of the MQ^+ reference compound from Figure 2b of the main paper and of its protonated congener (MQH^{2+}) was recorded in CH_3CN, pyridine, and in the pyridine / 0.22 M pyridinium mixture used for the spectroscopic studies. (**Figure S14**).

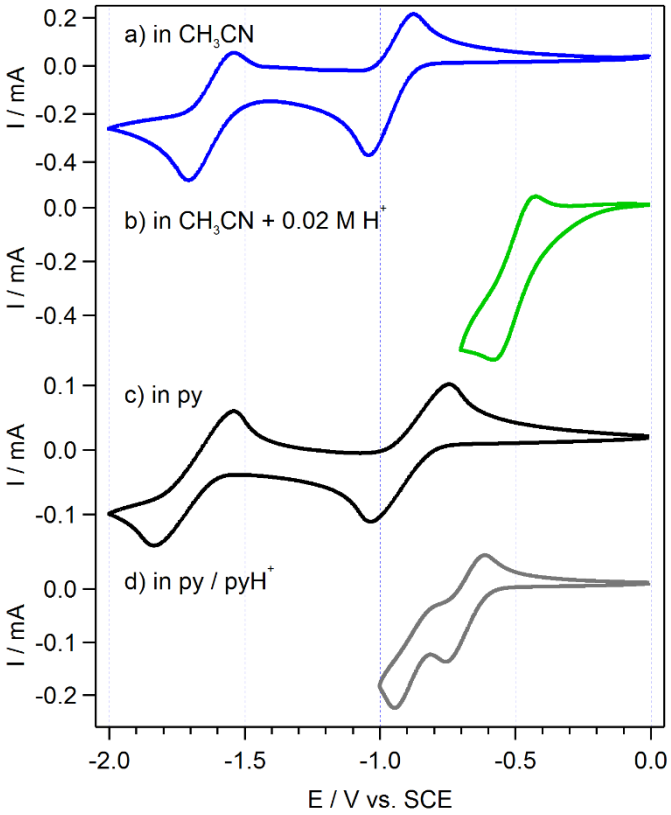

Figure S14. Cyclic voltammograms of MQ^+ and MQH^{2+} in CH_3CN, pyridine, and py / 0.22 M pyH^+ at potential sweep rates of 0.1 V s^{-1}.

The PCET thermodynamics of the 2,4,6-tri-*tert*-butylphenol donor unit have been reported previously for CH_3CN,[9] but not for pyridine solution and neither for the py / 0.022 M pyH^+ mixture. The cyclic voltammograms of 2,4,6-tri-*tert*-butylphenol in CH_3CN, pyridine, and py/pyH^+ are compared in **Figure S15**. No significant shift of oxidation potential is observed when changing the solvent from CH_3CN to pyridine or py / 0.022 M pyH^+.

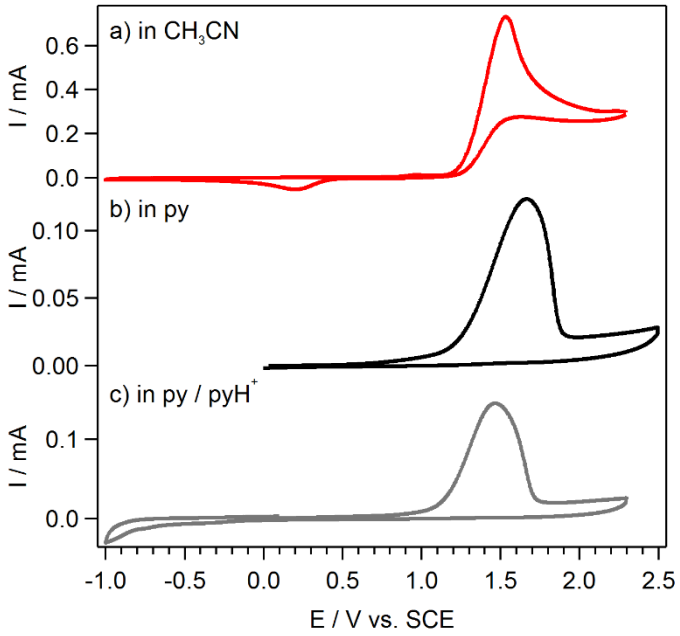

Figure S15. Cyclic voltammograms of 2,4,6-tri-*tert*-butylphenol in CH_3CN, pyridine, and py / 0.022 M pyH^+ at potential sweep rates of 0.1 V s^{-1}.

Table S3 presents an overview of the redox potentials of some key processes occurring at the PhOH donor and MQ^+ acceptor units of the triad based on the measurements in **Figure S14** and **Figure S15**.

Table S3. Relevant potentials for the triad (in V vs. SCE) in py and in py / 0.022 M pyH^+, based on measurements on reference molecules (**Figure S14** and **Figure S15**).

redox process	E [V]
$MQ^+ + py + e^- \rightarrow MQ^\bullet + py$	-0.89±0.1
$MQ^+ + pyH^+ + e^- \rightarrow MQH^{\bullet+} + py$	-0.68±0.1
$PhOH + py(H^+) \rightarrow PhOH^{\bullet+} + py(H^+) + e^-$	1.40 ±0.1

Summary of all relevant redox potentials and acidity constants

For the Ru(II) photosensitizer unit of the triad, the ground state redox potentials of $Ru(bpy)_3^{2+}$ were determined in pyridine (**Figure S13**). Excited state redox potentials were estimated on the basis of the known ^{3}MLCT energy and ground state redox potentials.[20] The relevant data is summarized in graphical form in **Figure S16**.

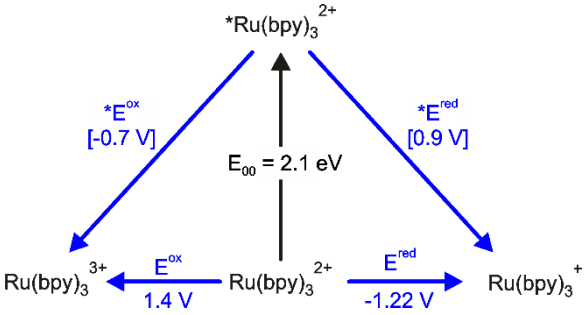

Figure S16. Latimer diagram for $Ru(bpy)_3^{2+}$ in pyridine. Potentials are given in Volts vs. SCE.

For the monoquat acceptor unit, the one-electron reduction potentials were determined in pyridine using the *N*-methyl-4,4'-bipyridinium (MQ^+) reference compound (**Figure S14c**, **Table S3**).

In addition, the electrochemical potential for reduction of MQ^+ in pyridine in presence of 0.22 M pyridinium was measured (**Figure S14d**). Under these conditions, one measures effectively the potential of the proton-coupled electron transfer (PCET) process leading from MQ^+ and pyH^+ to $MQH^{\bullet+}$ and py (or *vice versa*, green arrow in **Figure S17a**). From the respective potential (-0.68 V vs. SCE; **Table S3**), and the two relevant one-electron reduction potentials (-0.5 V vs. SCE, recorded in CH_3CN from **Table S1**, and -0.89 V vs. SCE, recorded in pyridine from **Table S3**) (blue arrows in **Figure S17a**) one can then estimate the reaction free energies for the proton transfer (PT) reactions represented by horizontal red arrows in the thermodynamic square scheme of **Figure S17a**. For example, the protonation of py by $MQH^{\bullet+}$ to afford pyH^+ and $MQ^\bullet$ is estimated to be endergonic by 0.21 eV based on this formalism. Using a pK_a value of 12.5 for pyridinium in CH_3CN,[10] this then translates to a pK_a value of 16 (= 12.5 + (0.21 V / 0.059 V)) for $MQH^{\bullet+}$ (top red arrow in **Figure S17b**). Similarly, a pK_a value of 9.4 (= 12.5 + (-0.18 V / 0.059 V)) is estimated for the MQH^{2+} species.

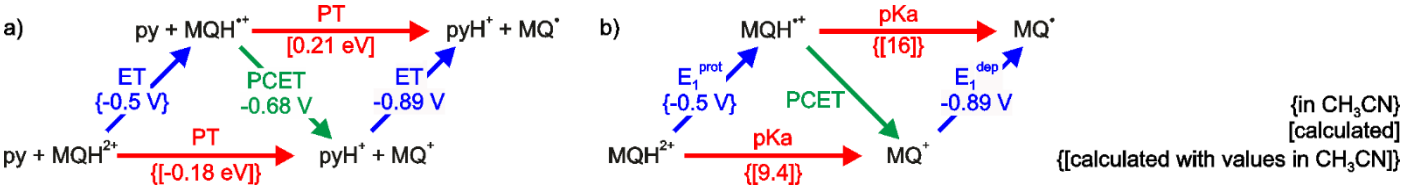

Figure S17. Thermochemical square scheme with all relevant redox potentials, driving forces, and acidity constants of the monoquat unit: (a) Redox potentials and driving-forces for proton transfer events. (b) Redox potentials and acidity constants derived from the data in (a) and the published pK_a value of pyH^+ in CH_3CN (12.5).[10] See text for details.

As noted above, 2,4,6-tri-*tert*-butylphenol was used as a reference compound to capture the redox and acid/base properties of the phenolic unit in the triad. The relevant thermochemical data for this compound have been reported previously for CH_3CN solution, and they are summarized in **Figure S18**.[9]

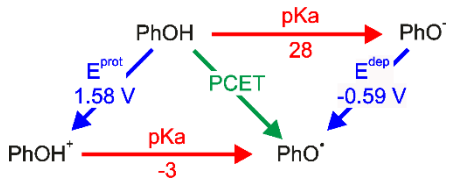

Figure S18. Thermochemical square scheme for 2,4,6-tri-*tert*-butylphenol (PhOH) in CH_3CN.[9] Redox potentials are given in V vs. SCE.

Using the data for pyridine/pyridinium solution from **Figure S15** (**Table S3**) and the published acidity constant of pyridinium in CH_3CN (pK_a = 12.5),[10] it becomes possible to estimate the relevant thermochemical parameters for 2,4,6-tri-*tert*-butylphenol in presence of pyridine. The respective data set is summarized in **Figure S19** in the form of a square scheme with redox potentials (blue arrows marked with ET; green arrow marked with PCET) and driving-forces for proton transfer (red arrows marked with PT).

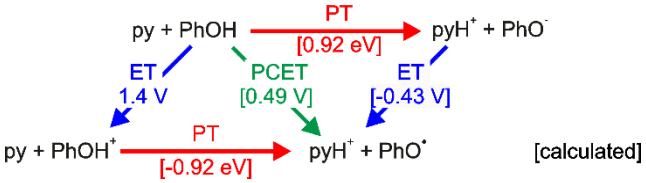

Figure S19. Thermochemical square scheme for 2,4,6-tri-*tert*-butylphenol (PhOH) in pyridine (py), estimated from pK_a values of PhOH and pyH^+ in CH_3CN and redox potential of phenolate in CH_3CN. Redox potentials are given in V vs. SCE.

A key outcome of this analysis is that the proton-coupled oxidation of PhOH occurs at substantially lower potential (0.49 V vs. SCE) than oxidation of PhOH to the phenoxyl radical cation (1.40 V vs. SCE).

Energy-level schemes based on relevant redox potentials and acidity constants

The lowest ^{3}MLCT excited state of the Ru(II) photosensitizer of the triad is assumed to be at the same energy (2.1 eV) as the emissive ^{3}MLCT state in $Ru(bpy)_3^{2+}$. The similarity of the luminescence spectrum in **Figure S4** on page S15 to the luminescence spectrum of $Ru(bpy)_3^{2+}$ supports this assumption. Thus, the initially excited state is at 2.1 eV:

(i) PhOH-$^*Ru^{2+}$-MQ^+ + py $E_1 = 2.1$ eV (eq. S10)

The $^*Ru^{2+}$ complex has a reduction potential of 0.9 V vs. SCE (**Figure S16** on page S27) and the PhOH unit has a one-electron oxidation potential of 1.40 V vs. SCE (**Figure S19** on page S28). Consequently, reductive quenching of $^*Ru^{2+}$ by PhOH to form Ru^+ and $PhOH^+$ is endergonic by 0.5 eV. Thus, $^*Ru^{2+}$ is not thermodynamically competent to oxidize PhOH without coupled proton release and the respective process is not a viable reaction pathway.
However, when phenol oxidation occurs in concert with proton release to pyridine base, then the relevant PCET redox potential is only 0.49 V vs. SCE (**Figure S19** on page S28). Consequently, reductive quenching of $^*Ru^{2+}$ becomes exergonic by ca. 0.4 eV in that case (eq. S11). Pyridinium (pyH^+) is formed as a side product. The resulting intermediate is at an energy of 1.7 eV (2.1 eV – 0.4 eV) above the electronic ground state (eq. S12).

PhOH-$^*Ru^{2+}$-MQ^+ + py → PhO$^\bullet$-Ru^+-MQ^+ + pyH^+ $\Delta G_{PCET} = -0.4$ eV (eq. S11)

(ii) PhO$^\bullet$-Ru^+-MQ^+ + pyH^+ $E_2 = 1.7$ eV (eq. S12)

Alternatively, oxidative quenching of $^*Ru^{2+}$ by MQ^+ must be considered. The oxidation potential of $^*Ru^{2+}$ is -0.7 V vs. SCE whereas the reduction potential of MQ^+ is -0.89 V vs. SCE (**Figure S16** and **Figure S17b** on page S27). Consequently, intramolecular electron transfer from $^*Ru^{2+}$ to MQ^+ is endergonic by ca. 0.2 eV (eq. S13). The respective photoproduct state is then 2.3 eV above the electronic ground state (eq. S14), and this is not a viable reaction pathway on thermodynamic grounds. Experimentally, this was shown with the Ru(II)-MQ^+ reference dyad in pyridine in **Figure S30** and **Figure S31** on page S39. The lifetime of the ^{3}MLCT state of the reference dyad in pyridine is 1090±109 ns and therefore comparable with the lifetime of ^{3}MLCT-$Ru(bpy)_3^{2+}$ in various solvents.[21]

PhOH-$^*Ru^{2+}$-MQ^+ + py → PhOH-Ru^{3+}-MQ$^\bullet$ + py $\Delta G_{ET} = +0.2$ eV (eq. S13)

(iii) PhOH-Ru^{3+}-MQ$^\bullet$ + py $E_3 = 2.3$ eV (eq. S14)

However, when MQ^+ reduction occurs in concert with protonation using 0.22 M pyridinium as an acid and pyridine as a solvent, then the relevant PCET redox potential is -0.68 V vs. SCE (**Figure S17b** on page S27). Consequently, oxidative quenching of $^*Ru^{2+}$ by MQ^+ via PCET is approximately ergoneutral (eq. S15) and the relevant photoproduct state is at roughly the same energy as the initial ^{3}MLCT state (eq. S16). The respective photo-experiment with the Ru(II)-MQ^+ reference dyad in py / 0.22 M pyH^+ shows only moderate quenching of the ^{3}MLCT state (τ = 300±30 ns) due to the presence of protons (**Figure S32** and **Figure S33** on page S40).

PhOH-$^*Ru^{2+}$-MQ^+ + pyH^+ → PhOH-Ru^{3+}-$MQH^{\bullet+}$ + py $\Delta G_{PCET} = 0.0$ eV (eq. S15)

(iv) $PhOH\text{-}Ru^{3+}\text{-}MQH^{\bullet+} + py$ $E_4 = 2.1$ eV (eq. S16)

As noted in the main paper, the most productive reaction pathway is therefore initial reductive $^{*}Ru^{2+}$ quenching by PhOH in a PCET reaction leading to state (ii) at 1.7 eV, in line with the H/D kinetic isotope effect of 2.2±0.2. Secondary intramolecular electron transfer from Ru^{+} to MQ^{+} is then exergonic by 0.3 eV (eq. S17), because the oxidation potential of Ru^{+} is -1.22 V vs. SCE whereas the one-electron reduction potential of MQ^{+} (to yield $MQ^{\bullet}$) is -0.89 V vs. SCE (**Figure S16** and **Figure S17b** on page S27).

$PhO^{\bullet}\text{-}Ru^{+}\text{-}MQ^{+} + pyH^{+} \rightarrow PhO^{\bullet}\text{-}Ru^{2+}\text{-}MQ^{\bullet} + pyH^{+}$ $\Delta G_{ET} = -0.3$ eV (eq. S17)

(v) $PhO^{\bullet}\text{-}Ru^{2+}\text{-}MQ^{\bullet} + pyH^{+}$ $E_5 = 1.4$ eV (eq. S18)

The acidity constant of pyH^{+} in CH_3CN is 12.5,[10] whereas the pK_a value of $MQH^{\bullet+}$ is 16 (**Figure S17b** on page S27). Consequently, there is ca. 0.2 eV (= 0.059 eV·(16-12.5)) driving-force for proton transfer from pyH^{+} to $MQ^{\bullet}$ in intermediate (v) (eq. S19), leading to the experimentally observable photoproduct state (vi) (eq. S20).

$PhO^{\bullet}\text{-}Ru^{2+}\text{-}MQ^{\bullet} + pyH^{+} \rightarrow PhO^{\bullet}\text{-}Ru^{2+}\text{-}MQH^{\bullet+} + py$ $\Delta G_{PT} = -0.2$ eV (eq. S19)

(vi) $PhO^{\bullet}\text{-}Ru^{2+}\text{-}MQH^{\bullet+} + py$ $E_6 = 1.2$ eV (eq. S20)

The decay pathways of this photoproduct are as follows. The oxidation potential of $MQH^{\bullet+}$ in CH_3CN is -0.5 V vs. SCE (**Figure S17b** on page S27), whereas the reduction potential of $PhO^{\bullet}$ in presence of py / pyH^{+} is -0.43 V vs. SCE (**Figure S19** on page S28). Consequently, there is ca. 0.1 eV driving-force for intramolecular electron transfer from $MQH^{\bullet+}$ to $PhO^{\bullet}$ yielding MQH^{2+} and PhO^{-} (eqs. S21/S22).

$PhO^{\bullet}\text{-}Ru^{2+}\text{-}MQH^{\bullet+} + py \rightarrow PhO^{-}\text{-}Ru^{2+}\text{-}MQH^{2+} + py$ $\Delta G_{ET} = -0.1$ eV (eq. S21)

(vii) $PhO^{-}\text{-}Ru^{2+}\text{-}MQH^{2+} + py$ $E_7 = 1.1$ eV (eq. S22)

The pK_a of MQH^{2+} in CH_3CN is 9.4 (**Figure S17b** on page S27), and the pK_a of PhOH is 28 in the same solvent (**Figure S18** on page S28).[9] Consequently, there is a driving-force of 1.1 eV (= 0.059 eV·(28-9.4)) for proton transfer between MQH^{2+} and PhO^{-} (eq. S23). Mechanistically, this occurs via protonation of py by MQH^{2+} and protonation of PhO^{-} by pyH^{+}, and the result is the initial ground state of the triad (eq. S24).

$PhO^{-}\text{-}Ru^{2+}\text{-}MQH^{2+} + py \rightarrow PhOH\text{-}Ru^{2+}\text{-}MQ^{+} + py$ $\Delta G_{PT} = -1.1$ eV (eq. S23)

(viii) $PhOH\text{-}Ru^{2+}\text{-}MQ^{+} + py$ $E_8 = 0.0$ eV (eq. S24)

Most estimates made above rely on redox potentials and acidity constants for CH_3CN solution due to lack of better alternatives. It seems more appropriate to use data for CH_3CN than for H_2O as approximated values for pyridine, due to the protic nature of H_2O. While some redox potentials are accessible for pyridine solution (page S25-S26), this is not the case for pK_a values.

Apparent photoacid behavior leading to phenolate formation in neat pyridine

Following excitation of the Ru(II) photosensitizer at 532 nm, its ^{3}MLCT excited state at 2.1 eV is rapidly populated. Based on the thermochemical data from **Figure S16** and **Figure S19**, the proton-coupled oxidation of PhOH by the ^{3}MLCT-excited photosensitizer ($^*Ru^{2+}$) in presence of pyridine (py) is exergonic by 0.4 eV:

$$PhOH\text{-}{}^*Ru^{2+}\text{-}MQ^+ + py \rightarrow PhO^{\bullet}\text{-}Ru^{+}\text{-}MQ^+ + pyH^+ \qquad \Delta G_{PCET} = -0.4\ eV \qquad \text{(eq. S11)}$$

For simplicity, Ru^+ denotes the reduced photosensitizer unit, but it should be kept in mind that its LUMO is ligand-based, and therefore this notation is not meant to reflect the metal oxidation state. According to **Figure S19**, the reduction of $PhO^{\bullet}$ to PhO^- occurs at a potential of -0.43 V vs. SCE, whereas oxidation of Ru^+ to Ru^{2+} occurs at -1.22 V vs. SCE (**Figure S16**). Consequently, intramolecular electron transfer from Ru^+ to $PhO^{\bullet}$ is exergonic by ca. 0.8 eV. This is a recombination-type side reaction of the photoinduced radical transfer in the triad:

$$PhO^{\bullet}\text{-}Ru^{+}\text{-}MQ^+ + pyH^+ \rightarrow PhO^{-}\text{-}Ru^{2+}\text{-}MQ^+ + pyH^+ \qquad \Delta G_{ET} = -0.8\ eV \qquad \text{(eq. S25)}$$

The product of this reaction is the phenolate species in its electronic ground state. We previously found the exact same type of photochemical mechanism, called apparent photoacid behavior, in a series of Ru(II)-phenol and Re(I)-phenol dyads.[1,22–24] (This photochemistry occurs only in a subset of triads in neat pyridine, while another subset reacts onward to produce the $PhO^{\bullet}\text{-}Ru^{2+}\text{-}MQ^{\bullet}$ photoproduct, leading to the $MQ^{\bullet}$ signature seen in Figure 2a of the main paper).
The phenolate photoproduct is only detectable in pyridine without triflic acid, because under these conditions the concentrations of $PhO^-\text{-}Ru^{2+}\text{-}MQ^+$ and pyH^+ are both equally low (< 10^{-5} M), hence the proton transfer from pyH^+ to PhO^- is slow even though it is strongly exergonic (eq. S26):

$$PhO^{-}\text{-}Ru^{2+}\text{-}MQ^+ + pyH^+ \rightarrow PhOH\text{-}Ru^{2+}\text{-}MQ^+ + py \qquad \Delta G_{PT} = -0.9\ eV \qquad \text{(eq. S26)}$$

The measured kinetics of the photochemistry described by equations S11, S25 and S26 (as measured in neat pyridine) is presented on page S33.

In the py / 0.22 M pyH^+ mixture, any phenolate species is more rapidly protonated by pyH^+ than it is formed, and consequently the PhO^- signature remains undetectable in presence of 0.22 M triflic acid in pyridine.

Optical absorption spectrum of the deprotonated triad in CH_3CN

The spectrum of the deprotonated triad was recorded in neat CH_3CN under inert atmosphere by adding 4 equivalents of tetrabutylammonium hydroxide (TBAOH) to the solution of the triad (**Figure S20**). The difference spectrum of the deprotonated triad in **Figure S21** was produced by subtracting the black trace from the red trace in **Figure S20**.

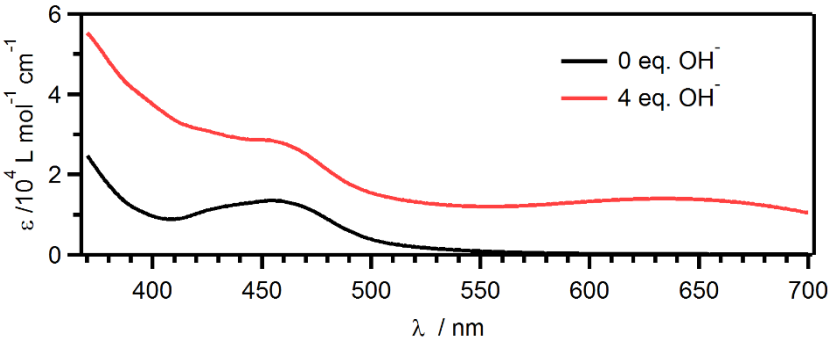

Figure S20. Optical absorption spectrum of the triad in CH_3CN (black trace) and upon addition of 4 equivalents of tetrabutylammonium hydroxide (TBAOH, red trace).

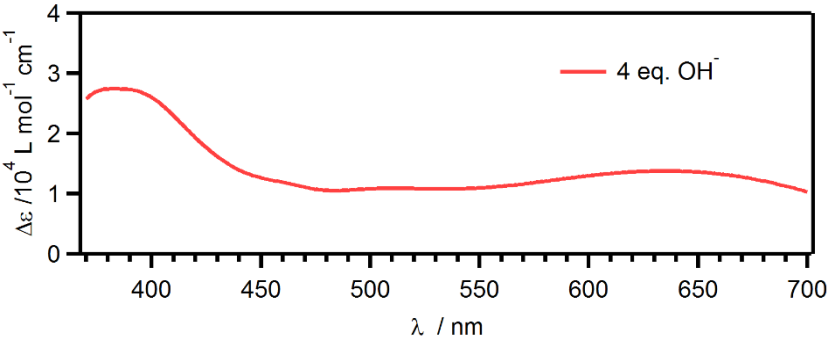

Figure S21. Difference absorption spectrum of the triad in CH_3CN upon deprotonation with 4 equivalents of TBAOH based on the absorption spectra in **Figure S20**.

The appearance of a difference band near 400 nm in **Figure S21** is taken as an indication for the formation of phenolate in the transient absorption spectrum from Figure 2a of the main paper recorded in neat pyridine (black trace).

Additional photochemical studies in neat pyridine without acid

Excitation of the triad in neat, de-aerated pyridine at 532 nm leads to the transient absorption spectra in **Figure S22**. These spectra were detected by time-integration over 200 ns after different delay times (see inset), following the 10-ns excitation pulses. The spectrum recorded with a delay of 2 μs corresponds to the black trace in Figure 2a of the main paper.

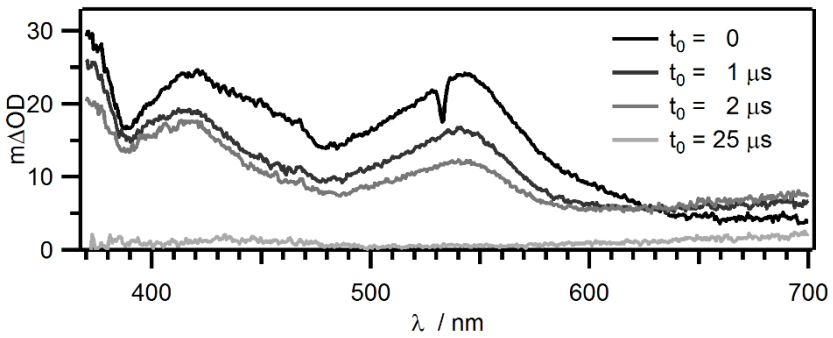

Figure S22. Transient absorption spectra of 55 μM triad in neat pyridine, recorded at different time delays (t_0) following excitation at 532 nm with laser pulses of ~10 ns duration.

The temporal evolution of the transient absorption signals at 3 different wavelengths (375, 420, 550 nm) are shown in **Figure S23** along with the ^{3}MLCT luminescence decay detected at 630 nm. Two different time axes are used to display rapid (left) and slow processes (right).

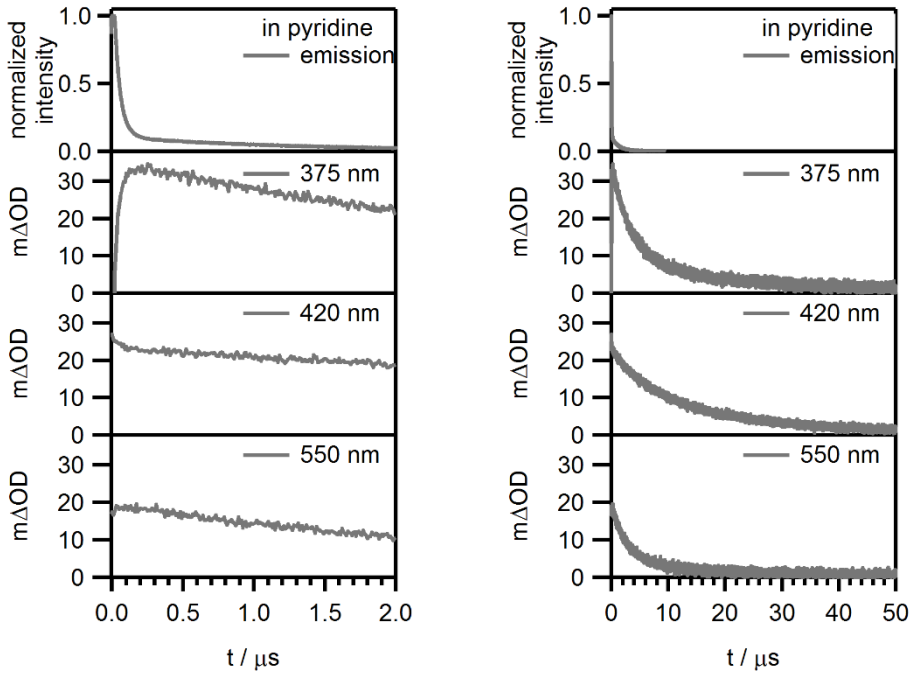

Figure S23. Kinetic traces for luminescence at 630 nm and transient absorption at 3 different wavelengths, recorded after excitation of 55 μM triad in neat pyridine at 532 nm. The laser pulse width was ~10 ns.

From the data in **Figure S22** and **Figure S23** one learns that the phenolate photoproduct PhO^{-}-Ru^{2+}-MQ^{+} is formed with a time constant of 35±4 ns (via the reaction described by equation S11 on page S31, followed by reverse electron transfer from Ru^{+} to $PhO^{\bullet}$; equation S25 on page S31). The PhO^{-}-Ru^{2+}-MQ^{+} photoproduct then decays with a time constant of 18±2 μs. Proton transfer between pyH^{+} and PhO^{-} (equation S26 on page S31) is so slow because the concentrations of these two reactants are both very low in neat pyridine ($< 10^{-5}$ M), as noted above.

The finding that in neat pyridine the photoproduct formation is faster than in the py/pyH^{+} mixture (τ = 35±4 ns vs. τ = 68±7 ns) is compatible with our mechanistic proposal from Scheme 1 of the main paper, in which reductive ^{3}MLCT quenching by PhOH with concerted proton release to pyridine is the rate-determining reaction step.

Photochemical studies in acetonitrile with pyrrolidine as base

Excitation of the triad at 532 nm in de-aerated acetonitrile in presence of 30 mM pyrrolidine leads to the transient absorption spectra in **Figure S24**. These spectra were detected by time-integration over 200 ns after different delay times (see inset), following the 10-ns excitation pulses.

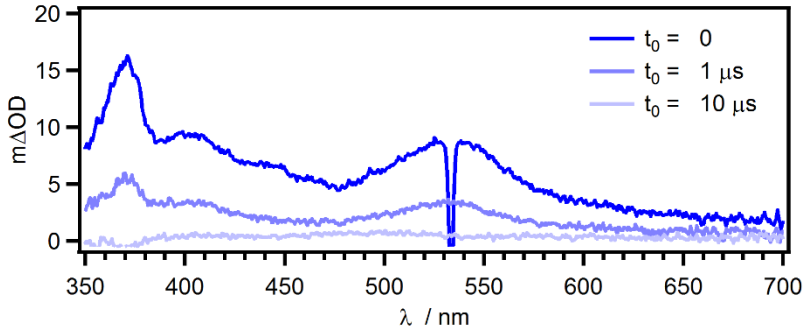

Figure S24. Transient absorption spectra of 47 µM triad in CH_3CN in presence of 30 mM pyrrolidine, recorded at different time delays (t_0) following excitation at 532 nm with laser pulses of ~10 ns duration.

The temporal evolution of the transient absorption signals at 3 different wavelengths (370, 405, 550 nm) are shown in **Figure S25** along with the ^{3}MLCT luminescence decay detected at 630 nm. Two different time axes are used to display rapid (left) and slow processes (right).

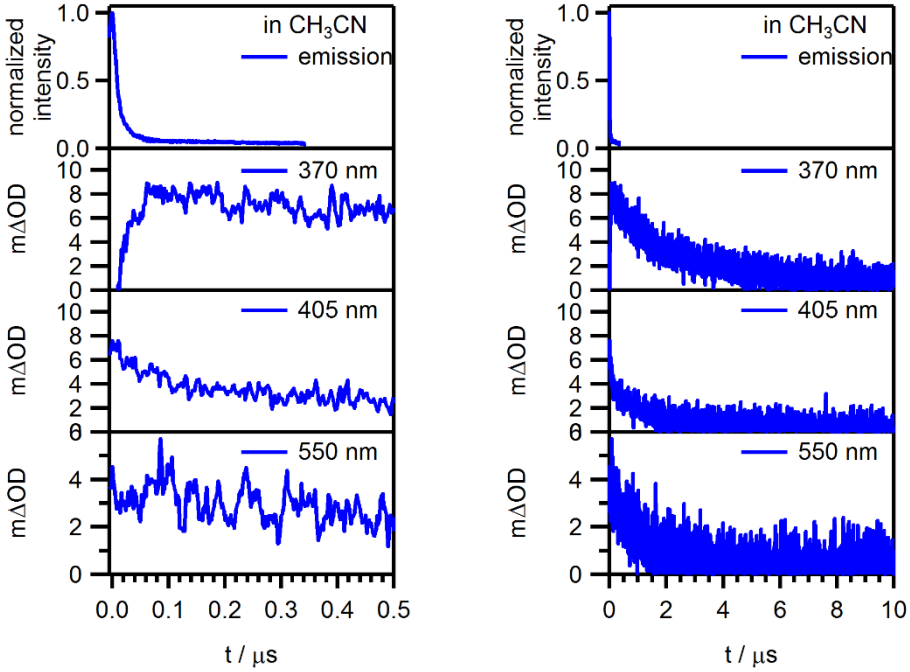

Figure S25. Kinetic traces for luminescence at 630 nm and transient absorption at 3 different wavelengths, recorded after excitation of 47 µM triad in CH_3CN in presence of 30 mM pyrrolidine at 532 nm. The laser pulse width was ~10 ns.

In CH_3CN and with 30 mM pyrrolidine, the luminescence of the triad is quenched to 12±1 ns. The generated radical decays with a lifetime of 1.5±0.2 µs. In CH_3CN, pyrrolidine (pK_a = 19.56) is a stronger base compared to pyridine (pK_a

= 12.53).[10] This can account for the observation of faster reaction kinetics in presence of pyrrolidine than in presence of pyridine (12±1 ns vs. 68±7 ns).

Optical spectroscopy of the Ru^{2+}-MQ^{+} reference dyad in CH_3CN, pyridine, and pyridine / pyridinium buffer

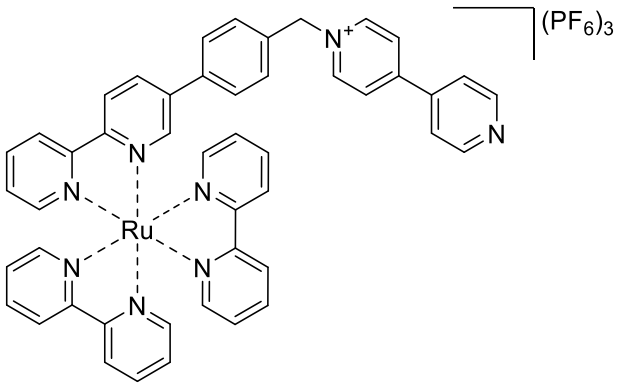

Ru^{2+}-MQ^{+}

Figure S26. The Ru^{2+}-MQ^{+} reference dyad.

The UV-Vis absorption spectra of the Ru(II)-MQ^{+} dyad in the solvents CH_3CN, pyridine, and pyridine / pyridinium are very similar (orange and gray traces in **Figure S27**).

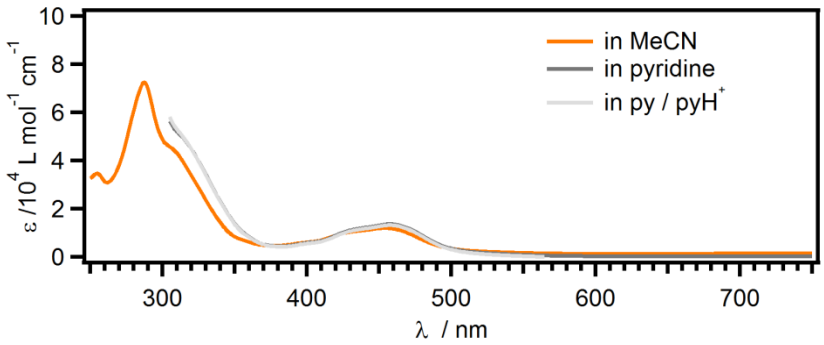

Figure S27. Optical absorption spectra of the Ru(II)-MQ^{+} dyad in CH_3CN (orange trace), pyridine (gray trace), and in py / 0.22 M pyH^{+}. At wavelengths shorter than 300 nm, pyridine is not sufficiently transparent hence the respective spectra are cut at this wavelength.

Excitation of the Ru(II)-MQ^{+} dyad in de-aerated CH_3CN at 532 nm with laser pulses of ~10 ns duration yields the spectrum shown in **Figure S28**. The signal was time-integrated over a period of 200 ns immediately after excitation.

This behavior is comparable to that of the triad, described in the main paper.

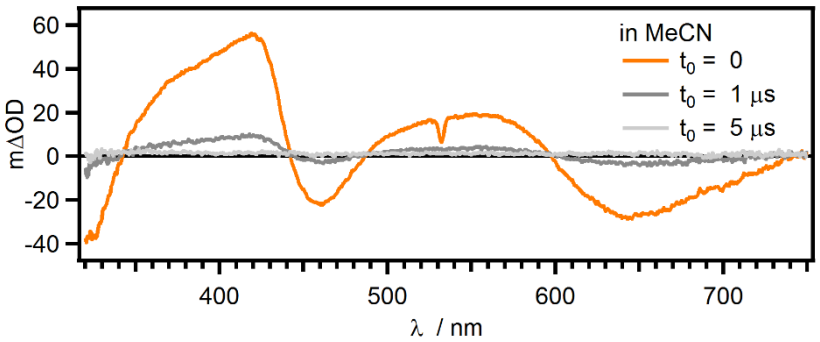

Figure S28. Transient absorption spectrum of 42 µM Ru(II)-MQ^+ dyad in de-aerated CH_3CN, recorded recorded after different time delays (t_0) following excitation at 532 nm with laser pulses of ~10 ns duration.

After pulsed excitation, the luminescence intensity at 630 nm decays with the same time constant as the transient absorption signals at 420 nm, 460 nm and 550 nm, namely with τ = 550±55 ns (**Figure S29**). Thus, no photochemistry occurs after excitation of the Ru(II)-MQ^+ dyad in neat CH_3CN, and there is merely ^{3}MLCT photoluminescence. The transient absorption spectrum in **Figure S28** is the signature of that ^{3}MLCT state.[7,8]

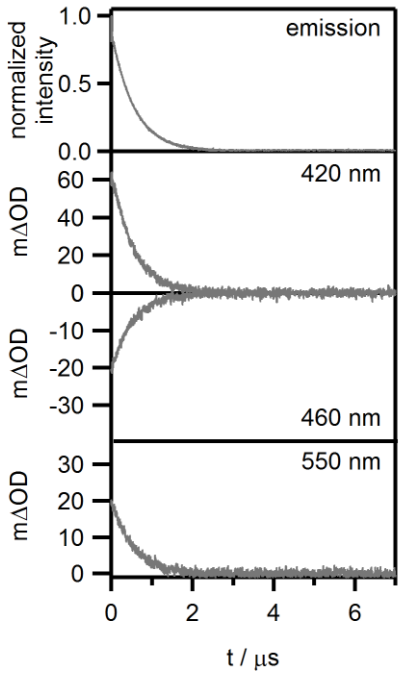

Figure S29. Kinetic data for 42 µM Ru(II)-MQ^+ dyad in de-aerated CH_3CN after excitation at 532 nm: Decay of the luminescence intensity at 630 nm, and decay of the transient absorption signals at 420 nm, 460 nm and 550 nm.

Excitation of the Ru(II)-MQ^+ dyad in neat, de-aerated pyridine at 532 nm with laser pulses of ~10 ns duration yields the transient absorption spectra shown in **Figure S30**. The signal was time-integrated over a period of 200 ns immediately after excitation, using different time delays (t_0) for detection.

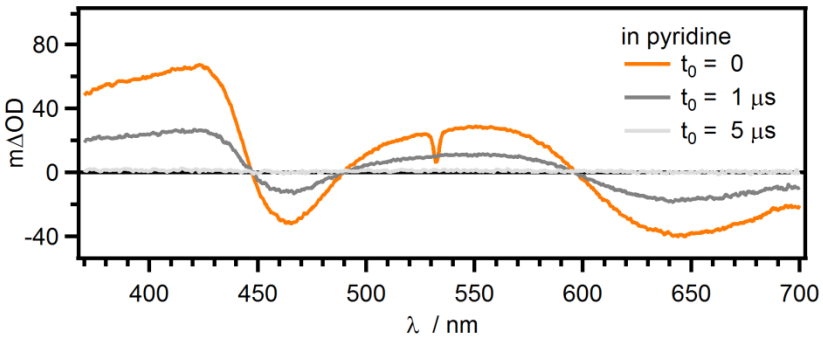

Figure S30. Transient absorption spectrum of 47 µM Ru(II)-MQ^+ dyad in neat, de-aerated pyridine, recorded after different time delays (t_0) following excitation at 532 nm with laser pulses of ~10 ns duration.

In de-aerated pyridine, the luminescence intensity at 630 nm decays with the same time constant as the transient absorption signals at 420 nm, 465 nm and 550 nm, namely with τ = 1090±109 ns (**Figure S31**). This lifetime is comparable with the lifetime of ^{3}MLCT-$Ru(bpy)_3^{2+}$ in various solvents.[21] Thus, no photochemistry occurs after excitation of the Ru(II)-MQ^+ dyad in neat pyridine, and there is merely ^{3}MLCT photoluminescence. The transient absorption spectra in **Figure S30** represent the signature of that ^{3}MLCT state.[7,8]

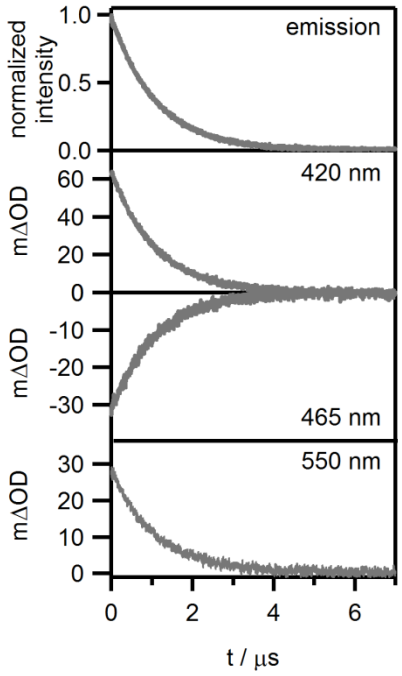

Figure S31. Kinetic data for 47 µM Ru(II)-MQ^+ dyad in neat, de-aerated pyridine after excitation at 532 nm: Decay of the luminescence intensity at 630 nm, and decay of the transient absorption signal at 420 nm, 465 nm and 550 nm.

Excitation of the Ru(II)-MQ^+ dyad at 532 nm in de-aerated pyridine with 0.22 M pyridinium using laser pulses of ~10 ns duration produced the spectra in **Figure S32**. The signals were time-integrated over a period of 200 ns after excitation using different time delays for detection.

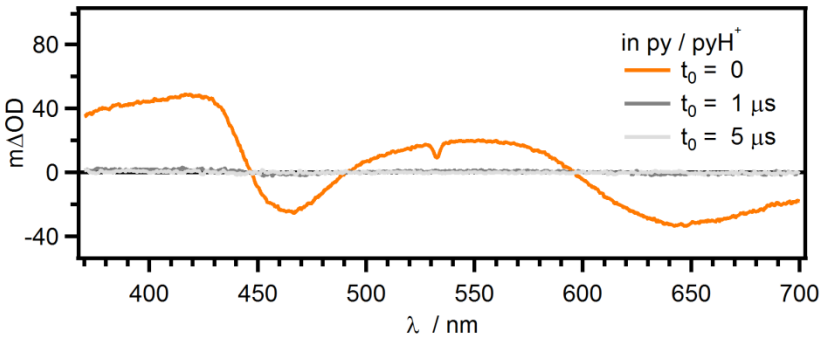

Figure S32. Transient absorption spectra of 47 µM Ru(II)-MQ^+ dyad in de-aerated pyridine with 0.22 M pyridinium, recorded after different time delays (t_0) following excitation at 532 nm with laser pulses of ~10 ns duration.

Similar to what is observed in neat CH_3CN as well as in neat pyridine without pyridinium, the luminescence intensity at 630 nm decays with the same time constant (τ = 300±30 ns) as the transient absorption signals at 420 nm, 465 nm and 550 nm (**Figure S33**). Moreover, the orange trace in **Figure S32** strongly resembles the ^{3}MLCT difference spectra observed in **Figure S28** and **Figure S30**, and therefore we conclude that in the pyridine / pyridinium buffer the observable spectral signature is that of the ^{3}MLCT excited state. However, compared to neat pyridine in which the ^{3}MLCT lifetime is 1090±109 ns (see above), the ^{3}MLCT decay is faster in pyridine / pyridinium buffer by approximately a factor of 3. This weak quenching is attributed to photoinduced electron transfer from the photoexcited Ru(II) sensitizer to MQ^+ coupled to protonation of the latter, owing to the presence of pyridinium. Based on the relevant redox potentials and acidity constants, this reaction is approximately ergoneutral (equation S15 on page S29). The electron transfer products remain undetectable, most likely because they recombine to the starting materials by reverse thermal electron transfer more rapidly than they are formed. This is a common observation for such dyads, and in particular for several previously investigated $Ru(bpy)_3^{2+}$-methyl viologen donor-acceptor compounds.[25–29]

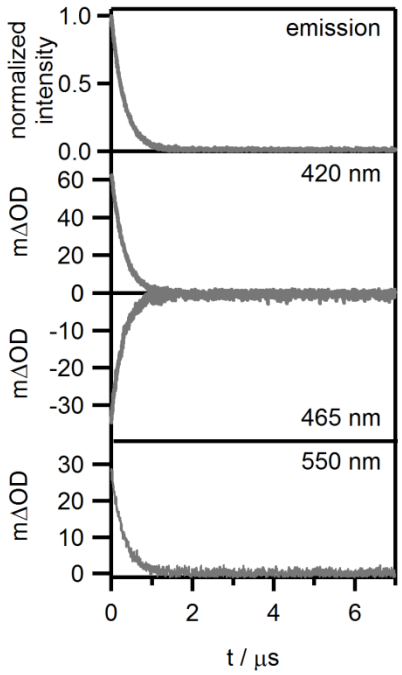

Figure S33. Kinetic data for Ru(II)-MQ^+ dyad in neat, de-aerated pyridine after excitation at 532 nm: Decay of the luminescence intensity at 630 nm, and decay of the transient absorption signal at 420 nm, 465 nm and 550 nm.

Photoreaction versus ^{3}MLCT relaxation and quantum yield for photoproduct formation in the triad

Photoexcitation of the triad in the py / 0.22 M pyH^+ mixture leads to biphasic luminescence decays as shown in Figure 3a of the main paper. The major decay component (68±7 ns; 85%) was attributed unambiguously to the formation of the main photoproduct based on complementary transient absorption data (Figure 3b/c in the main article), whereas the minor luminescence decay component (780±80 ns; 15%) is compatible with ^{3}MLCT decay pathways encountered also in the isolated $Ru(bpy)_3^{2+}$ complex with no attached donors or acceptors. Thus, ~15% of all excited triad molecules do not undergo photoreaction.

As discussed above, the hydrogen-bonding association between pyridine and PhOH in CH_3CN is rather weak, and an association constant of 0.16±0.04 M^{-1} was determined by ^{1}H NMR titrations (pages S19 - S20). Even in neat pyridine-d_5 not all PhOH molecules seem to be hydrogen-bonded. Presumably, this is due to the sterically demanding *tert*-butyl substituents in *ortho*-position of the hydroxyl group. In earlier studies, this fact even permitted X-ray crystallographic characterization of the 2,4,6-tri-*tert*-butylphenoxyl radical.[16] Thus, it seems plausible that also in the py / 0.22 M pyH^+ mixture a substantial proportion of phenolic units are not hydrogen-bonded, and consequently the respective triad molecules are not predisposed to undergo photochemical reactions. In particular, proton-coupled oxidation of PhOH (identified in the main paper as the rate-determining step in photoproduct formation) is not readily possible for these molecules.

Analysis of the transient absorption data in terms of assessing the quantum yield for photoproduct formation leads to a similar conclusion, as discussed in the following.

The transient absorption spectrum of the triad in neat CH_3CN (**Figure S3** on page S15) exhibits the typical ^{3}MLCT signature of the Ru(II) photosensitizer. Since the sensitizer in the molecular ensemble of the triad has attached *p*-xylene and phenylene units with donor and acceptor moieties on one of the three bpy ligands, the two main absorption bands of this ^{3}MLCT spectrum are somewhat red-shifted with regard to their positions in $Ru(bpy)_3^{2+}$.[7] Specifically, the band observed at 580 nm in **Figure S3** corresponds to the absorption band at 450 nm of ^{3}MLCT-excited $Ru(bpy)_3^{2+}$, whereas the more intense band observed at 440 nm in **Figure S3** corresponds to the band at 385 nm in the ^{3}MLCT spectrum of $Ru(bpy)_3^{2+}$.[7] Similar red-shifts of the ^{3}MLCT absorption bands of a Ru(II) sensitizer incorporated into molecular triads have been observed previously.[8] At 450 nm, ^{3}MLCT-excited $Ru(bpy)_3^{2+}$ has an extinction coefficient of $4.6 \cdot 10^3$ M^{-1} cm^{-1}, and given the spectral analogy with red-shifts discussed above, we assume that the ^{3}MLCT-excited Ru(II) photosensitizer at 580 nm has the same extinction coefficient.[7] On this basis we determine a concentration of 2.5 μM for ^{3}MLCT-excited triad under the conditions used to record the data in **Figure S3**. This corresponds to ~9% of the total triad concentration (27 μM) in the respective sample.

Using the transient absorption data recorded from the triad in the py / 0.22 M pyH^+ mixture (green trace in Figure 2a of the main paper) and extinction coefficients of $2.5 \cdot 10^4$ M^{-1} cm^{-1} at 400 nm and $5.5 \cdot 10^3$ M^{-1} cm^{-1} at 600 nm for the $MQH^{\bullet+}$ unit (assumed to be identical to the extinction coefficients of methyl viologen radical at the respective absorption band

maxima in DMF),[14] we estimate that the concentration of $PhO^{\bullet}$-Ru^{2+}-$MQH^{\bullet+}$ photoproduct in this solution is 2.7 μM. Given a triad concentration of 34 μM in this sample, this corresponds to ~8% photoproduct formation.

Taken together, these experiments indicate that under the typical conditions used for our transient absorption studies, ~9% of the present triad molecules are excited to the ^{3}MLCT state of the photosensitizer (in CH_3CN), and ~8% of the present triad molecules react to the $PhO^{\bullet}$-Ru^{2+}-$MQH^{\bullet+}$ photoproduct (in py / pyH^+ mixture). From this one can conclude that the quantum yield for photoproduct formation out of the ^{3}MLCT excited state is ~90%. This finding is in line with the analysis of the ^{3}MLCT luminescence decay behavior made above with 15% non-reacting ^{3}MLCT states due to absence of hydrogen bonding to the phenolic proton.

Given the approximations regarding extinction coefficients described above and given the fact that two separate experiments have to be compared, the quantum yield estimate is associated with considerable error bars. However, in combination with the ^{3}MLCT luminescence decay analysis from above this approach becomes reasonably trustworthy.

Dynamic shift of the acid-base equilibrium between phenol and pyridine

As noted on page S17, the phenolic unit of the PhOH-Ru^{2+}-MQ^+ triad in pyridine is in an acid-base equilibrium with the solvent:

$$PhOH + py \leftrightarrows PhO^- + pyH^+ \qquad \text{(eq. S1)}$$

The law of mass action for this reaction is:

$$K = \frac{[pyH^+]\cdot[PhO^-]}{[PhOH]\cdot[py]} \qquad \text{(eq. S2)}$$

As noted above, the equilibrium constant K can be calculated from the acidity constants of PhOH (pK_{a1}) and pyH^+ (pK_{a2}) according to eq. S3. We use the following values for CH_3CN solution: $pK_{a1} = 28$,[9] $pK_{a2} = 12.5$.[10]

$$K = 10^{-\Delta pKa} = 10^{-(pKa1-pKa2)} = 10^{-(28-12.5)} = 10^{-15.5} \qquad \text{(eq. S3)}$$

For chemical reactions involving a single step, the following relationship between equilibrium constant K and rate constants for forward (k_f) and backward (k_b) reactions is valid:

$$K = k_f / k_b \qquad \text{(eq. S27)}$$

Assuming the rate for protonation of PhO^- by pyH^+ is diffusion-limited ($k_b = 10^{11}\ M^{-1}\ s^{-1}$), it follows for the rate constant for deprotonation (k_f) of PhOH by pyridine:

$$k_f = K \cdot k_b = 10^{-15.5} \cdot 10^{11}\ M^{-1}\ s^{-1} = 10^{-4.5}\ M^{-1}\ s^{-1} \qquad \text{(eq. S28)}$$

The molarity of neat pyridine is ca. 12 M. The pseudo first-order rate constant for phenol deprotonation then becomes:

$$k_f = 10^{-4.5}\ M^{-1}\ s^{-1} \cdot 12\ M \approx 10^{-3}\ s^{-1} \qquad \text{(eq. S29)}$$

Thus, the pseudo first-order rate constant for PhOH deprotonation is ca. 10 orders of magnitude slower than the rate constant for photoproduct formation observed for the PhOH-Ru(II)-MQ^+ triad in py/pyH^+ ($\tau = 68\pm7$ ns; $\tau^{-1} \approx 1.5\cdot10^7\ s^{-1}$). This is incompatible with a dynamic shift of the equilibrium in eq. S1 after photoexcitation, and it excludes the possibility of a proton transfer, electron transfer sequence (PT-ET) for $PhO^\bullet$ formation after excitation of the triad.

The estimation of k_f relies on acidity constants for CH_3CN, because pK_a values for neat pyridine are not available. For the comparison with the experimentally observed rate constant this procedure seems entirely reasonable in view of the resulting very large difference in rate constants (10 orders of magnitude; $1.5\cdot10^7\ s^{-1}$ vs. $10^{-3}\ s^{-1}$). The difference in pK_a

values between PhOH and pyH^+ would have to become at least 8 logarithmic units smaller in neat pyridine than in CH_3CN in order for the key conclusion drawn here to become questionable.

References

(1) Kuss-Petermann, M.; Wolf, H.; Stalke, D.; Wenger, O. S. *J. Am. Chem. Soc.* **2012**, *134*, 12844.

(2) Hankache, J.; Wenger, O. S. *Chem. Commun.* **2011**, *47*, 10145.

(3) Liu, S.-J.; Zhao, Q.; Chen, R.-F.; Deng, Y.; Fan, Q.-L.; Li, F.-Y.; Wang, L.-H.; Huang, C.-H.; Huang, W. *Chem. Eur. J.* **2006**, *12*, 4351.

(4) Fang, Y.-Q.; Hanan, G. S. *Synlett* **2003**, *2003*, 852.

(5) Sullivan, B. P.; Salmon, D. J.; Meyer, T. J. *Inorg. Chem.* **1978**, *17*, 3334.

(6) Pannwitz, A.; Wenger, O. S. *Phys. Chem. Chem. Phys.* **2016**, *18*, 11374.

(7) Yoshimura, A.; Hoffman, M. Z.; Sun, H. *J. Photochem. Photobiol. A Chem.* **1993**, *70*, 29.

(8) Kuss-Petermann, M.; Wenger, O. S. *Angew. Chem., Int. Ed.* **2016**, *55*, 815.

(9) Warren, J. J.; Tronic, T. A.; Mayer, J. M. *Chem. Rev.* **2010**, *110*, 6961.

(10) Kaljurand, I.; Kütt, A.; Sooväli, L.; Rodima, T.; Mäemets, V.; Leito, I.; Koppel, I. A. *J. Org. Chem.* **2005**, *70*, 1019.

(11) Nomrowski, J.; Wenger, O. S. *Inorg. Chem.* **2015**, *54*, 3680.

(12) Macomber, R. S. *J. Chem. Educ.* **1992**, *69*, 375.

(13) Biczok, L.; Gupta, N.; Linschitz, H. *J. Am. Chem. Soc.* **1997**, *119*, 12601.

(14) Braterman, P. S.; Song, J. I. *J. Org. Chem.* **1991**, *56*, 4678.

(15) Ishida, H.; Ohba, T.; Yamaguchi, T.; Ohkubo, K. *Chem. Lett.* **1994**, *23*, 905.

(16) Manner, V. W.; Markle, T. F.; Freudenthal, J. H.; Roth, J. P.; Mayer, J. M. *Chem. Commun.* **2008**, *246*, 256.

(17) Gadosy, T. A.; Shukla, D.; Johnston, L. J. *J. Phys. Chem. A* **1999**, *103*, 8834.

(18) Das, P. K.; Encinas, M. V.; Steenken, S.; Scaiano, J. C. *J. Am. Chem. Soc.* **1981**, *103*, 4162.

(19) Brede, O.; Orthner, H.; Zubarev, V.; Hermann, R. *J. Phys. Chem.* **1996**, *100*, 7097.

(20) Roundhill, D. M. *Photochemistry and Photophysics of Metal Complexes*; Plenum Press: New York, 1994.

(21) Juris, A.; Balzani, V.; Barigelletti, F.; Campagna, S.; Belser, P.; von Zelewsky, A. *Coord. Chem. Rev.* **1988**, *84*, 85.

(22) Kuss-Petermann, M.; Wenger, O. S. *J. Phys. Chem. Lett.* **2013**, *4*, 2535.

(23) Chen, J.; Kuss-Petermann, M.; Wenger, O. S. *Chem. Eur. J.* **2014**, *20*, 4098.

(24) Bronner, C.; Wenger, O. S. *Phys. Chem. Chem. Phys.* **2014**, *16*, 3617.

(25) Lomoth, R.; Häupl, T.; Johansson, O.; Hammarström, L. *Chem. Eur. J.* **2002**, *8*, 102.

(26) Henrich, J. D.; Zhang, H. Y.; Dutta, P. K.; Kohler, B. *J. Phys. Chem. B* **2010**, *114*, 14679.

(27) Yonemoto, E. H.; Saupe, G. B.; Schmehl, R. H.; Hubig, S. M.; Riley, R. L.; Iverson, B. L.; Mallouk, T. E. *J. Am. Chem. Soc.* **1994**, *116*, 4786.

(28) Mecklenburg, S. L.; Peek, B. M.; Schoonover, J. R.; McCafferty, D. G.; Wall, C. G.; Erickson, B. W.; Meyer, T. J. *J. Am. Chem. Soc.* **1993**, *115*, 5479.

(29) Kelly, L. A.; Rodgers, M. A. J. *J. Phys. Chem.* **1995**, *99*, 13132.